

# **SPECTRAL INVESTIGATIONS OF THERMALLY STABLE RARE EARTH EMBEDDED ZINC BOROPHOSPHATE GLASSES FOR OPTOELECTRONIC APPLICATIONS**

A DISSERTATION SUBMITTED  
IN PARTIAL FULFILMENT OF THE REQUIREMENTS FOR THE DEGREE

OF  
**MASTER OF SCIENCE**  
IN  
**PHYSICS**



Submitted by  
**Mr. Tushar Singh**  
**(23/MSCPHY/88)**

*Under the Joint Supervision of*

**Dr. M. Jayasimhadri**  
Associate Professor  
Department of Applied Physics  
Delhi Technological University  
Delhi-110 042

**Dr. K. Pavani**  
Research Professor  
Department of Physics & I3N  
University of Aveiro, 3810-193,  
Portugal

**DEPARTMENT OF APPLIED PHYSICS**  
**DELHI TECHNOLOGICAL UNIVERSITY**  
**BAWANA ROAD, DELHI-110 042, INDIA**

June, 2025



# DELHI TECHNOLOGICAL UNIVERSITY

Formerly Delhi College of Engineering

(Under Delhi Act 6 of 2009, Govt. of NCT of Delhi)

Shahbad Daultapur, Bawana Road, Delhi-110 042

## CANDIDATE'S DECLARATION

I **Mr. Tushar Singh, (Roll No. 23/MSCPHY/88)** hereby certify that the work which is presented in the Dissertation entitled "*Spectral Investigations of Thermally Stable Rare Earth Embedded Zinc Borophosphate Glasses for Optoelectronic Applications*" in partial fulfillment of the requirements for the award of the **Degree of Master of Science in Physics**, submitted in the Department of Applied Physics, Delhi Technological University, Delhi is an authentic record of my own work carried out during the period from July 2024 to June 2025 under the joint supervision of **Dr. M. Jayasimhadri**, Department of Applied Physics, Delhi Technological University, Delhi and **Dr. K. Pavani**, Department of Physics & I3N, University of Aveiro, Portugal.

The matter presented in this report has not been submitted and is not under consideration for the award for any other course/degree of this or any other Institute/University. The work has been communicated in peer reviewed/ Scopus-indexed conference and journal with the following details:

**Title of the Paper (I):** Spectral Investigations of Thermally Stable Rare Earth Embedded Zinc Borophosphate Glasses for Optoelectronic Applications

**Author names (in the sequence as per research paper):** Tushar Singh, Vertika Siwach, M. Jayasimhadri, K. Pavani

**Name of Conference:** International Conference on Emerging Materials and Quantum Photonics (ICEMQP-2024)

**Name of the Journal:** Springer Proceedings (Scopus Indexed)

**Conference Dates with venue:** 2024, November 07-09, GJU Hisar (Haryana)

**Have you registered for the conference:** Yes

**Status of paper (Accepted/ Published/ Communicated):** Accepted

**Date of paper communication:** May, 2025

**Tushar Singh**  
(23/MSCPHY/88)

## SUPERVISOR CERTIFICATE

To the best of my knowledge, the above work has not been submitted in part or full for any Degree or Diploma to this University or elsewhere. I, further certify that the publication and indexing information given by student is correct.

Place: Delhi

Date: 9 June 2025

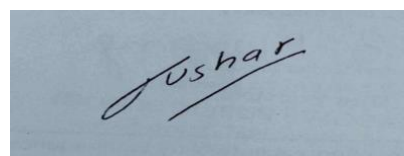
  
Dr. M. Jayasimhadri

**Dr. M. Jayasimhadri**  
Supervisor & Associate Professor  
Department of Applied Physics  
Delhi Technological University  
Delhi-110 042, India

**Dr. K. Pavani**  
Joint-supervisor & Research Professor  
Department of Physics & I3N  
University of Aveiro  
Aveiro- 3810-193, Portugal

## ACKNOWLEDGEMENTS

I would like to convey my heartfelt thanks to **Dr. M. Jayasimhadri**, Associate Professor, Department of Applied Physics, Delhi Technological University, Delhi and **Dr. K Pavani**, Department of Physics & I3N, University of Aveiro, Portugal for allowing me to work under their supervision and for providing me with continual inspiration and unwavering support throughout the project. I'd like to take this occasion to thank my supervisors for their passionate assistance, knowledge, fantastic ideas, useful comments, and consistent support. I am appreciative of the continual assistance and convenience provided by all lab members (Ph.D. scholars), especially **Dr. Vikas Sangwan** and **Ms. Vertika Siwach**, Dept. of Applied Physics, at every stage of my study. Furthermore, I have been fortunate and thankful to my family and friends for their love, and care, as they patiently extended all kinds of assistance to help me complete this duty.

A handwritten signature in black ink on a light blue background. The signature is written in a cursive style and appears to read 'Tushar'.

**Tushar Singh**  
**(23/MSCPHY/88)**

## ABSTRACT

Zinc borophosphate (NBZPB) glasses embedded with various  $\text{Pr}^{3+}$  ion concentrations were formed through a melt quenching procedure. Thermal, structural, optical, and photoluminescent (PL) features of those glasses were thoroughly studied in detail. Differential scanning calorimetry (DSC) analysis was employed to assess the thermal stability of the glass host composition. X-ray diffraction (XRD) profiles were utilized to verify the non-crystalline nature of the formed glasses. The optical qualities of the formed NBZPBPr glass matrices were computed with the help of the optical absorption profiles. Furthermore, when stimulated with blue radiation of 446 nm wavelength, the emission profiles of the formed NBZPBPr glasses exhibit an intense orange-red emission (602 nm) in the visible region. The chromaticity characteristics, including color coordinates ( $x$ ,  $y$ ), color purity (CP) and correlated color temperature (CCT), of the optimized glass were examined under selected blue excitation. Moreover, the temperature dependent photoluminescence (TDPL) analysis demonstrated that the titled glass matrix has excellent thermal stability. The findings mentioned above confirm that the formed NBZPBPr glasses could be a potential candidate for optoelectronic applications.

## **TABLE OF CONTENTS**

<i>Title Page</i> .....	<i>i</i>
<b>Candidate's Declaration</b> .....	<b><i>ii</i></b>
<b>Acknowledgments</b> .....	<b><i>iii</i></b>
<b>Abstract</b> .....	<b><i>iv</i></b>
<b>Table of Contents</b> .....	<b><i>v</i></b>
<b>List of Abbreviations</b> .....	<b><i>vii</i></b>
<b>List of Figures &amp; Tables</b> .....	<b><i>viii</i></b>
<b>Chapter -1: Introduction</b> .....	<b>1-17</b>
<b>1.1. Introduction and motivation</b> .....	<b>1</b>
<b>1.2. History</b> .....	<b>3</b>
<b>1.3. Definition of glass</b> .....	<b>4</b>
<i>1.3.1. Components of glass</i> .....	<i>5</i>
<i>1.3.2. Glass preparation methods</i> .....	<i>8</i>
<b>1.4. Luminescence</b> .....	<b>9</b>
<i>1.4.1. Types of Luminescence</i> .....	<i>9</i>
<i>1.4.2. Photoluminescence: Phosphorescence and Fluorescence</i> .....	<i>11</i>
<b>1.5. Rare-Earth Elements</b> .....	<b>13</b>
<i>1.5.1. Characteristics of Rare Earth Ions</i> .....	<i>14</i>
<b>1.6. White light LEDs</b> .....	<b>15</b>
<i>1.6.1. Methods to generate White Light</i> .....	<i>16</i>
<b>Chapter -2: Experimental and Characterization Techniques</b> .....	<b>18-28</b>

<b>2.1. Selection of Host Materials.....</b>	<b>18</b>
<b>2.2. Synthesis Procedure.....</b>	<b>19</b>
<b>2.3. Characterization Techniques.....</b>	<b>20</b>
<b>2.3.1 Thermal Analysis.....</b>	<b>21</b>
<b>2.3.2 X-ray Diffraction (XRD).....</b>	<b>21</b>
<b>2.3.3 Fourier Transform Infrared (FT-IR) Spectroscopy.....</b>	<b>23</b>
<b>2.3.4 Optical Absorption Spectral Analysis.....</b>	<b>25</b>
<b>2.3.5 Photoluminescence Spectroscopy (PL).....</b>	<b>26</b>
<b>2.3.6 Temperature Dependent PL Spectroscopy (TDPL).....</b>	<b>28</b>
 <b>Chapter-3: Results and Discussion.....</b>	 <b>31-41</b>
<b>3.1. Thermal Analysis- TGA-DSC.....</b>	<b>31</b>
<b>3.2. Structural Analysis- XRD and FT-IR.....</b>	<b>32</b>
<b>3.3. Absorption Spectral Profiles.....</b>	<b>34</b>
<b>3.4. Luminescent Studies- PL and PLE.....</b>	<b>36</b>
<b>3.5. Colorimetric Studies.....</b>	<b>40</b>
<b>3.6. Temperature Dependent PL Analysis.....</b>	<b>41</b>
 <b>Chapter-4: Conclusion and Future Scope.....</b>	 <b>43</b>
<b>4.1. Conclusions.....</b>	<b>43</b>
<b>4.2. Future Scope of the Work.....</b>	<b>43</b>
<b>References.....</b>	<b>44-51</b>

## **List of Abbreviations**

LED	Light emitting diodes
w-LEDs	White light emitting diodes
RE	Rare earth
Pr	Praseodymium
TGA-DSC	Thermogravimetric Analysis-Differential Scanning Calorimetry
XRD	X-ray Diffraction
FT-IR	Fourier Transform Infrared
PL	Photoluminescence
CIE	Commission Internationale de l'Éclairage
CCT	Correlated Color Temperature
CP	Color Purity
TDPL	Temperature Dependent PL

## List of Figures

Figure No.	Figure Captions	Page No.
1.1	<i>Timeline of LEDs.</i>	3
1.2.	<i>General volume changes associated with heating and cooling in systems susceptible to glass formation.</i>	8
1.3.	<i>Classification Of Luminescence.</i>	10
1.4.	<i>Rare earth ions and their electronic configurations.</i>	13
1.5.	<i>Three common ways to generate White light.</i>	16
2.1.	<i>Melt Quenching Method Diagram.</i>	20
2.2.	<i>The Sataram Labsys Evo instrument.</i>	21
2.3.	<i>Bragg's Diagram.</i>	22
2.4.	<i>High-resolution X-ray diffractometer.</i>	23
2.5.	<i>Schematic Working Diagram of FT-IR.</i>	24
2.6.	<i>V-770 UV-Visible/NIR Spectrophotometer up to 3200 nm.</i>	26
2.7	<i>Shimadzu RF-5301 PC spectrofluorophotometer with a Xenon (150 W) bulb.</i>	27
2.8.	<i>Ocean Optics (FLAME-S-XR1-ES) Spectrophotometer.</i>	28
2.9.	<i>Labelled Diagram of TD-PL Spectrofluorometer.</i>	29



3.1.	<i>Differential scanning calorimetry (DSC) for the NBZPB glass host.</i>	31
3.2.	<i>X-ray diffraction (XRD) profiles for the NBZPB host and NBZPBPr<sub>0.1</sub> glasses.</i>	32
3.3.	<i>FT-IR spectrum for the NBZPB host glass.</i>	33
3.4.	<i>Optical absorption spectrum of 0.1 mol% Pr<sup>3+</sup> doped NBZPB glass sample in the n-UV-VIS-NIR region. [Inset signifies the indirect allowed band gap energy of the NBZPBPr<sub>0.1</sub> glass sample using Tauc's plot].</i>	34
3.5.	<i>PLE spectrum for the NBZPBPr<sub>0.1</sub> glass with fixed 602 nm emission wavelength.</i>	37
3.6	<i>PL spectra for the Pr<sup>3+</sup> doped NBZPBPr glass samples for excitation at <math>\lambda_{\text{ex}} = 446</math> nm. The inset plot shows the variation of PL intensity of the emission peak (<math>^1D_2 \rightarrow ^3H_4</math>) with varying Pr<sup>3+</sup> concentration ions in NBZPB glasses.</i>	37
3.7.	<i>Partial Energy level scheme for the Pr<sup>3+</sup> doped NBZPB glass samples.</i>	39
3.8.	<i>CIE chromaticity Plot of the NBZPBPr<sub>0.1</sub> glass under 446 nm excitation wavelength.</i>	40
3.9.	<i>Temperature-dependent PL spectra for the optimized NBZPBPr<sub>0.1</sub> glass sample with temperature varying from 303 K to 473 K under 446 nm excitation wavelength. [Inset represents the relative emission intensity variation with varying temperatures from 303 K to 473 K.</i>	41
3.10.	<i>Linear fitted plot between <math>\ln[(I_0/I_T) - 1]</math> versus <math>1/K_B T</math>.</i>	42

## Chapter-1: Introduction

---

### 1.1. Introduction and Motivation

With the advancement of modern civilization, the rapidly growing demand for energy consumption and its environmental effects, including greenhouse gas emissions, have concerned researchers for a long time [1]. About 1900 million tonnes (Mt) of carbon dioxide (CO<sub>2</sub>) emissions are caused by lighting annually. About 80% of these emissions connected to lighting are caused by the production of electricity. However, about 20% comes from burning paraffin and oil-based fuels directly, which are mostly used by the 1.6 billion people who do not yet have access to electricity worldwide. Approximately 650 Mt of primary energy is consumed globally for lighting, and lighting technologies are responsible for more than 20% of global electricity consumption and 7% of global CO<sub>2</sub> emissions. In order to lessen the environmental impact of traditional lighting systems, these figures highlight the pressing need for more ecologically friendly and energy-efficient lighting technology [2-4].

Solid-state lighting represents a transformative paradigm shift in illumination technologies, characterized by the replacement of conventional incandescent and fluorescent sources with devices based on semiconductor principles such as light-emitting diodes (LEDs) and organic light-emitting diodes (OLEDs) [5, 6]. SSL has emerged in response to global energy challenges and environmental concerns, primarily due to its significantly lower power consumption, extended lifetime, and superior spectral control when compared with traditional lighting sources [7, 8, 9]. The evolution of SSL technologies has been driven by the twin incentives of reducing greenhouse gas emissions through lower electrical energy consumption and providing a sustainable solution for both residential and commercial settings [10]. Solid State Lighting based on semiconductor light emitting diodes (LED) offers long-lasting life, is

highly efficient, gives high quality colour rendering and lower energy consumption compared to traditional lighting methods such as incandescent lamps and fluorescent lamps [11-14]. Nowadays, LEDs can achieve more than 50% energy to light conversion [15, 16]. Commercially acclaimed are the solid-state White light emitting diodes (WLEDs) and in commercial W-LED lighting, a combination of  $\text{Y}_3\text{Al}_5\text{O}_{12}:\text{Ce}^{3+}$  yellow phosphor with blue LED chip and epoxy resin is typically utilized to produce white light [17-19]. WLEDs based on the phosphor conversion model require epoxy resin or silica gel as binding materials at the interface of the chip-phosphor [18, 20]. These epoxy resins are made up of polymer/organic materials that have many disadvantages, including rapid wear, poor colour index, low heat dissipation efficiency, reduced transmissivity due to uneven refractive index, yellowing and carbonization of phosphor caused by heating and ageing [21]. Their deterioration at elevated temperatures demonstrates lower thermal stability, leading to additional declines in both the colour rendering index and luminous efficiency of LEDs and however, achieving the right balance of the three coloured phosphors is quite challenging, and the production cost could be significantly elevated [22]. Therefore, Luminescent glasses are introduced as a new substitute material for phosphor. Luminescent glasses are in an advantageous position in good thermal stability, excellent luminescent efficiency, high uniformity, and elevated doping concentration of rare-earth ions (RE ions) [19, 23, 24]. Eliminating the need for epoxy resin lowers production cost, simplifies the manufacturing process, has high luminous efficacy, lower correlated colour temperature (CCT) and high colour rendering index (CRI) properties and achieves good transparency [18, 25, 26]. Luminescent glasses have the potential to act as encapsulating material for the generation of white LEDs [19, 24].

In an effort to develop a superior luminescent material, rare earth (RE) doped composites have recently been the subject of intensive investigation. RE ion emissions generally originate from optical transitions within the  $f$ -manifold [27]. The triple-ionized state of RE ions causes them

to stimulate electromagnetic radiation in the visible to near-infrared (NIR) spectrum [28]. Among all the trivalent  $RE^{3+}$  ions, praseodymium ( $Pr^{3+}$ ) ions are the most preferred for simultaneously exploiting visible emissions (blue, orange, and red) and specific infrared regions, due to the presence of discrete emitting energy levels, such as metastable levels like  $^1G_4$ ,  $^1D_2$ , and  $^3P_{2,1,0}$ , etc. [29-32].

## 1.2. History

LED technology development represents a long and arduous scientific journey that transformed early findings of electroluminescence into a versatile, high-performance, energy-efficient light source. Early pioneering experiments in the 1900s with materials such as silicon carbide ignited the first interest in studying light emission from semiconductors. The development of functional p–n junctions, the separation between direct and indirect bandgap materials, and the development of the first visible LEDs in the 1960s set the basis for the modern era.

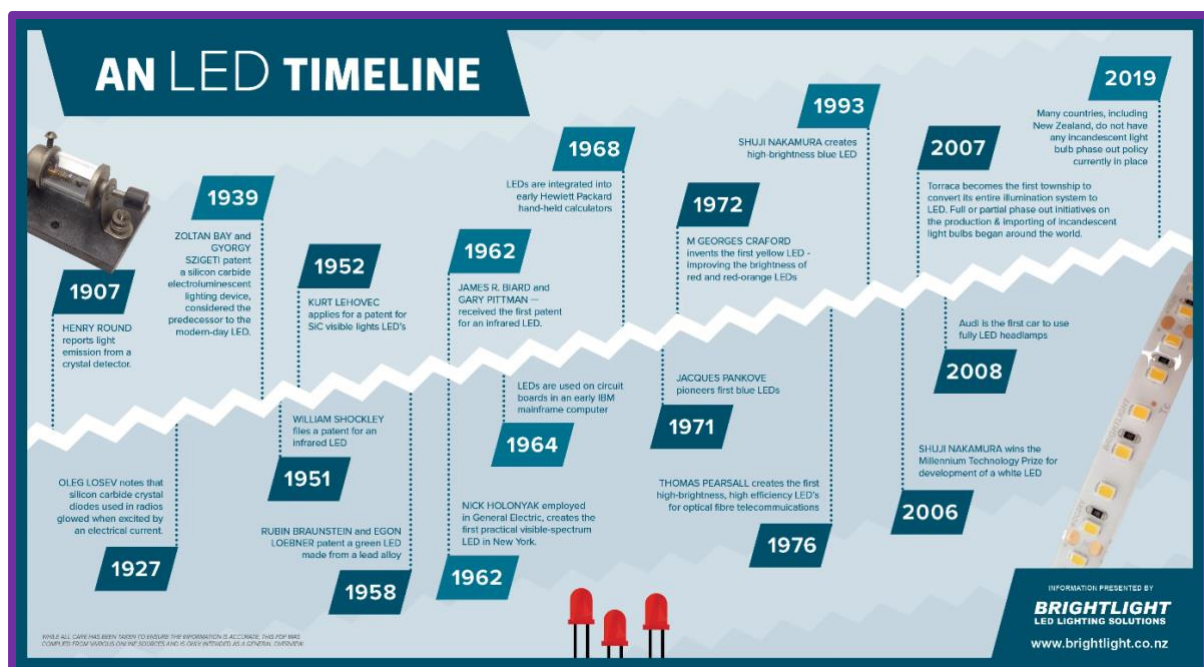


Fig. 1.1. Timeline of LEDs.

Developments in producing high-quality GaN-based blue LEDs by scientists such as Akasaki, Amano, and Nakamura triggered great leaps in device efficiency and production scalability, hence enabling the commercialization of white LEDs and the solid-state lighting revolution. Advances in epitaxial growth techniques, innovative chip architectures, and innovative packaging methods have continued to improve LED efficiency and intensity. The integration of LEDs into many applications, general lighting, dental photopolymerization, agriculture, and biomedical imaging, demonstrates the profound impact of LED technology on many aspects of life today. As the field continues to develop, continued advancements in device engineering and materials science will likely uncover new uses and enhance the performance of these already revolutionary devices [33-35].

### **1.3. Definition of glass**

Glass is conventionally defined as when a melt is cooled quickly enough to avoid crystallization, the liquid state is arrested into a stiff, disordered form, resulting in glass, which is traditionally defined as an amorphous solid with no long-range periodicity in its atomic structure [36]. Transparency, toughness, chemical inertness, and heat resistance are just a few of glass's advantageous qualities. Because of these qualities, it can be used in a variety of fields, such as electronics, art, packaging, and construction. Once primarily considered an optical and passivating medium, glass can be utilized to create active devices such as switches, sensors, solar cells, etc [37]. Although traditional definitions such as those by ASTM emphasize glass as an inorganic product formed by fusion and cooled without crystallization, modern scientific perspectives extend this definition to include organic or metallic glasses produced by a variety of methods, thereby focusing on the inherent amorphous state and the observable glass transition phenomenon rather than solely on the method of synthesis .

### ***1.3.1. Components of Glass***

The functions and properties of glass are significantly influenced by its constituent parts. Glass displays a distaste for crystal in a random network. Glass components are categorized into three classes: network modifiers, glass network formers, and intermediates, each with varying binding strengths. Some other important components are flux, colorant and fining agent. Understanding the components of glass is essential for both fundamental research and the development of applications ranging from consumer products to high-technology devices. Glass, despite its amorphous nature, is constructed from a mixture of chemical oxides and additional modifiers that define its short-range and intermediate-range order in the absence of long-range periodicity.

- ***Glass Formers:*** Glass formers are materials or components that can form glass when cooled from a molten state without crystallizing. They are essential components of glass because they provide its characteristic non-crystalline or amorphous structure. Glass formers such as  $\text{SiO}_2$ ,  $\text{B}_2\text{O}_3$ ,  $\text{P}_2\text{O}_5$ ,  $\text{V}_2\text{O}_5$ ,  $\text{As}_2\text{O}_3$ ,  $\text{PO}_4$ ,  $\text{GeO}_2$ ,  $\text{Sb}_2\text{O}_5$ , and others are widely utilized and significant. The glass skeleton can be formed by these oxides alone. In glass network formers, the cations-oxygen coordination number is typically four.
- ***Network modifiers:*** Glass modifiers break the normal link between oxygen and glass-forming ingredients by loosely attaching themselves to oxygen atoms. The primary function of the network modifiers is to alter the features of the glass. Most glass modifiers consist of alkali oxides. Alkaline oxides and network modifiers alter the characteristics of glass. A few significant network modifiers are the oxides  $\text{K}_2\text{O}$ ,  $\text{Li}_2\text{O}$ ,  $\text{Na}_2\text{O}$ ,  $\text{BaO}$ ,  $\text{SrO}$ ,  $\text{CaO}$ , and  $\text{MgO}$ . Choosing the right cation-oxide modifier was necessary for the most recent uses of glasses, including bioactive materials, sensors, optoelectronics, lasers, and lighting systems.

- ***Intermediates:*** In order to connect with the core glass network and preserve structural continuity, glass intermediates, mostly metal oxides, are added. The intermediaries are positioned between the glass formers and the modifiers. Some significant examples of intermediates include the oxides  $\text{Al}_2\text{O}_3$ ,  $\text{TiO}_2$ ,  $\text{CdO}$ ,  $\text{PbO}$ ,  $\text{BeO}$ , and  $\text{ZnO}$ . The words "glass formers," "intermediaries," and "modifiers" are typically used to describe the specific oxides in a multicomponent glass host system. Based on the composition of the glass host matrix, the intermediate oxides in the glass can act as both network formers and network modifiers.
- ***Colorent:*** The final glass's color is controlled with colorants. Colorants are typically oxides of either the 4f rare earths or the 3d transition metals. Gold and silver are also used to produce colors via the formation of colloids in glasses. Colorants are often present in small quantities and are only utilized when control over the glass's color is wanted.

To encourage the elimination of bubbles from the melt, fining agents are added to batches of glass being formed. Arsenic and antimony oxides, potassium and sodium nitrates,  $\text{NaCl}$ , fluorides like  $\text{CaF}_2$ ,  $\text{NaF}$ , and  $\text{NaAlF}_4$ , and many sulfates are examples of fining agents. These substances are typically found in extremely small amounts (less than 1 weight percent) and are typically handled as though their impact on the finished glasses' characteristics is negligible. Nonetheless, they are necessary for the production of many commercial glasses, which would be unaffordable without the use of fining agents to lower the amount of undesirable bubbles in the finished product [38].

***Glass Transition:*** Every glass that forms within the temperature range called the "glass transformation region" exhibits time-dependent behavior in glass transformation. Glass Transition Temperature ( $T_g$ ) is a fundamental thermal parameter that characterizes the

temperature range over which amorphous materials, such as polymers, food matrices, and other non-crystalline substances, transition from a hard, glassy, brittle state to a softer, rubbery, or viscous state as temperature increases [39]. The rate at which each substance cools produces a different glass. Glass is produced when a material is rapidly cooled from a supercooled liquid. The substance is lowered below the so-called glass-transition temperature to produce an amorphous solid. After that, when the atoms begin to move more slowly in a molecular pattern, the substance begins to transform into glass. Although the newly formed non-crystalline structure is less ordered than a crystal, it is nevertheless more ordered than a liquid. When a liquid is cooled below its melting point without undergoing crystallization, it enters a supercooled state. In this state, the atomic structure of the liquid continues to reorganize as the temperature drops, but no sharp drop in enthalpy occurs because there's no sudden structural change. As cooling progresses, the liquid's viscosity increases significantly. Eventually, the viscosity becomes so high that the atoms can no longer fully rearrange into their equilibrium positions within the time frame of the experiment. As a result, the structure begins to lag what would be expected under equilibrium conditions.

At this stage, the enthalpy starts to diverge from the equilibrium path, following a curve with a progressively decreasing slope. This continues until the enthalpy is determined solely by the heat capacity of the immobilized structure. At this point, the liquid's structure is effectively "frozen", no longer dependent on temperature and behaves as a glass. The temperature range between the equilibrium liquid's enthalpy and that of the rigid, non-equilibrated structure is referred to as the **glass transition region**, and the resulting material is called a **glass**.

The temperature at which the enthalpy diverges from the equilibrium path is influenced by the liquid's viscosity, a kinetic factor. If the cooling rate is reduced, the system has more time to approach equilibrium, allowing the enthalpy to follow the equilibrium curve down to a



lower temperature. This shifts the glass transition region to a lower temperature, and the resulting glass will have a lower enthalpy compared to one formed through rapid cooling. Consequently, the atomic structure of the more slowly cooled glass corresponds to the equilibrium liquid structure at a lower temperature than that of the rapidly cooled one.

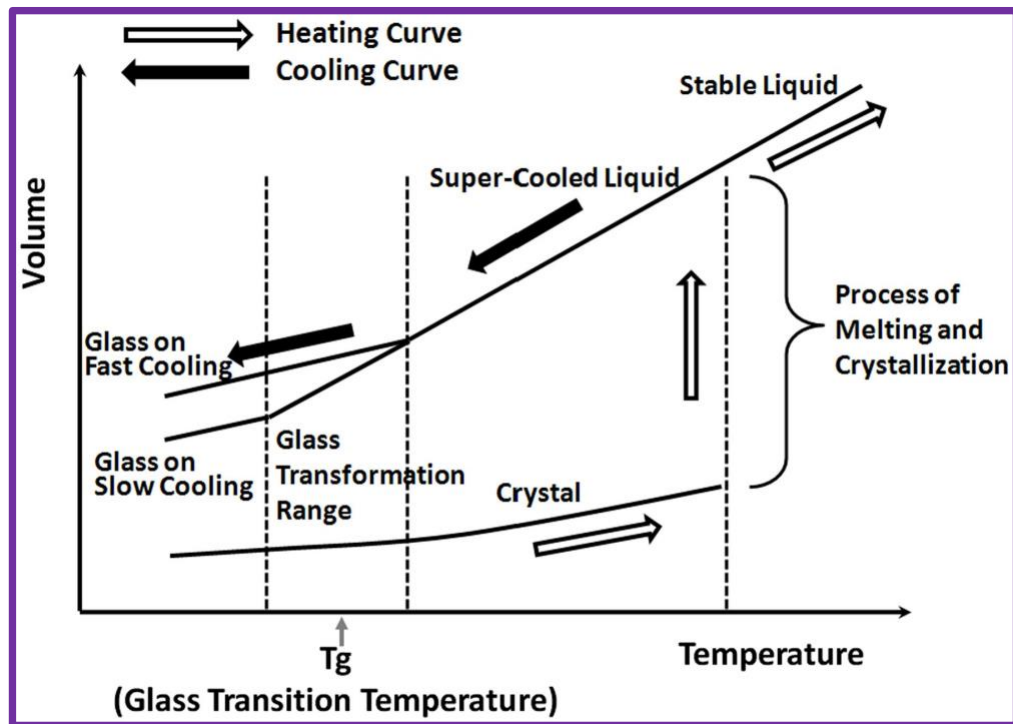


**Fig. 1.2.** General volume changes associated with heating and cooling in systems susceptible to glass formation.

### 1.3.2. Glass Preparation Methods

Depending on the planned application of the glass sample and the intended analysis or experiment, different preparatory stages may be required.

- Thermal Evaporation
- Melt Quenching
- Sol-gel Method
- Chemical Vapor Deposition

- Chemical Reaction
- Electrolytic Deposition

The Melt Quenching is the easiest and widely utilized procedure.

## 1.4. Luminescence

Luminescence is caused by non-thermal processes that occur at normal and lower temperatures[40, 41]. It is distinct from incandescence, which is light generated by the energy of heat [40]. Luminescent materials are materials that exhibit this phenomenon [40].

Luminescence is a process in which energy excites an electron from the ground state into an excited or higher state; then the electron thus emits optical radiation (in the visible spectra region or the infrared region) with lower energy (down-converted) [40, 41].

Luminescence originates when electrons are excited from lower energy states (often the valence band in inorganic solids) to higher energy states, such as the conduction band or discrete excited states provided by impurity levels or trap centers, and then return to the ground state through radiative recombination.

### 1.4.1. Types of Luminescence:

- **Electroluminescence:** light generated when an electric field is applied in a gas or solid by emitting visible photons. Source: Electric field.
- **Chemiluminescence:** energy released by chemical reaction causes light emission. Source: Chemical reaction
- **Photoluminescence (PL):** caused by excitation and de-excitation by absorption of electromagnetic radiation or a photon. Source: Photons

- **Cathodoluminescence:** caused by electron beam emission when electron beams excite phosphor material. Applications in LCDs, cathode ray tubes and scanning electron microscopy (SEM). Source: Electron beam

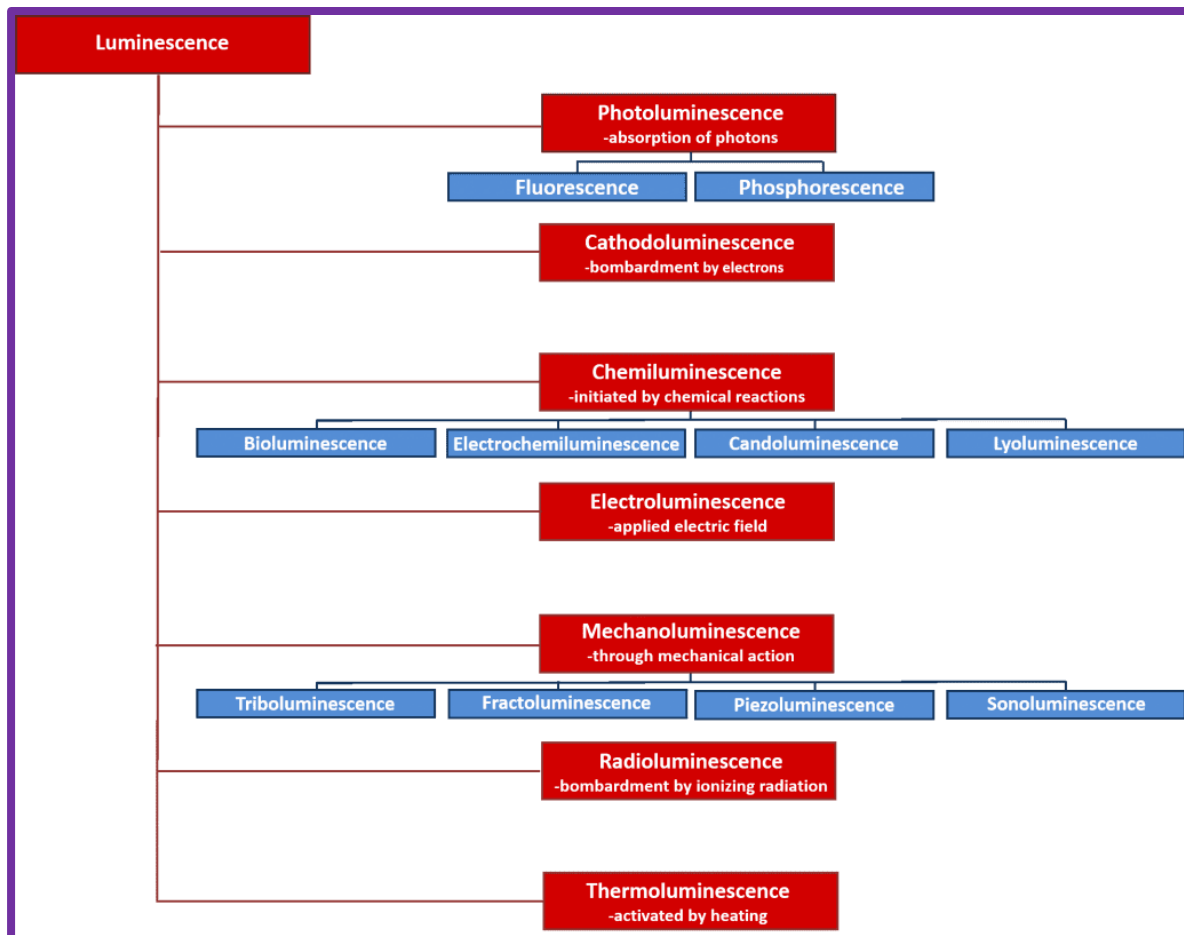


**Fig.1.3.** *Classification Of Luminescence.*

- **Thermoluminescence:** when a luminescent material after being excited by radiation is thermally heated. Source: Heat
- **Radioluminescence:** luminescence produced by the effect of being radiated by ionizing radiation for instance x-rays, beta or gamma rays. Source: X-rays
- **Bioluminescence:** occurs in deep waters where light is produced by chemical reactions by living organisms. Source: Biochemical Reaction

- ***Triboluminescence:*** Mechanical tension causes luminescence known as mechanoluminescence. Source: Mechanical stress to crystals or by the Fracture of crystals.
- ***Sonoluminescence:*** luminescence produced by ultrasonic wave excitation. Source: Rapid implosion of cavitation bubbles in a liquid, triggered by strong sound waves (ultrasound) [42].

#### ***1.4.2. Photoluminescence: Phosphorescence and Fluorescence***

The well-known photoluminescence is the process by which the activator absorbs the energy of electromagnetic radiation as photons, followed by subsequent emission in the visible spectrum. Activators are the ions that interact with the luminescence center in the host matrix.

In general, the photoluminescence occurs in three steps:

- The activator relaxes to the excited state's lowest energy state;
- The activator is excited from its ground/lower energy state to a higher energy level.
- Photons are emitted when activator ions transition from the excited state to the ground state.

There are two approaches to classifying PL according to emission or decay time.

- ***Fluorescence:*** When a substance absorbs energy from an external source, such as ultraviolet (UV) radiation, it quickly reemits that energy as visible light. The emission rapidly stops when the excitation source is removed. Fluorescence occurs in photoluminescence (PL) when emission happens within  $10^{-8}$  seconds after the excitation source is withdrawn. Visible photons are rapidly emitted as electrons move from an excited state to a distinct ground state energy level [43]

- **Phosphorescence:** The primary difference between fluorescence and phosphorescence is the delay in light emission from the phosphor even after the excitation source has been turned off. After being absorbed as light over an extended period of time, the material continues to radiate energy when the excitation source is removed. After some time spent near a light source, glow-in-the-dark stickers and other phosphorescent materials continue to produce light. Phosphorescent materials emit a glow that can last from a few minutes to several hours as the excited electrons gradually return to their ground state. Thus, phosphorescence is another name for the delayed fluorescence process .

### Process:

- **Absorption:** When incident light with energy equal to or greater than the semiconductor's bandgap is absorbed, electrons from the valence band are promoted into the conduction band, forming hole-electron pairs or excitons. This process starts with photon absorption [44].
- **Excitation:** Electrons are excited from the ground or defect states to either discrete excitonic states in low-dimensional systems or to delocalized conduction band states [45].
- **Non-Radiative Relaxation:** Upon excitation, excess excited carriers rapidly lose energy through non-radiative processes, such as phonon emission, surface or defect state interactions, before radiative recombination occurs [46].
- **Emission-** Radiative recombination is the process by which electrons and holes recombine to release their excess energy in the form of photons, manifesting as the photoluminescence signal [47].

## 1.5. Rare-Earth Elements

Rare earth ions, also known as lanthanoid ions, exhibit a unique combination of chemical, optical, magnetic, and catalytic properties that underpin their critical role in advanced materials science and modern technology. Their shielded 4f electron systems confer narrow absorption and emission bands, long luminescence lifetimes, and stable redox behavior independent of the host matrix. Rare earth elements, comprising the fifteen lanthanides along with scandium and yttrium, are distinguished by their nearly identical chemical behavior and unique electronic configurations, which arise from the partially filled 4f orbitals shielded by filled 5s and 5p subshells. This electronic shielding is responsible for the narrow, well-defined optical transitions that are minimally affected by the host environment and provide exceptional luminescence properties [48].

4f-block elements (lanthanides)							
Valence shell electronic Configuration $4f^{0,2 \text{ to } 14} 5d^{0,1} 6s^2$							
57 <b>La</b> lanthanum 138.905 $4f^0 5d^1 6s^2$	58 <b>Ce</b> Cerium 140.116 $4f^2 5d^0 6s^2$	59 <b>Pr</b> Praseodymium 140.908 $4f^3 5d^0 6s^2$	60 <b>Nd</b> Neodymium 144.243 $4f^4 5d^0 6s^2$	61 <b>Pm</b> Promethium 144.913 $4f^5 5d^0 6s^2$	62 <b>Sm</b> Samarium 150.360 $4f^6 5d^0 6s^2$	63 <b>Eu</b> Europium 151.964 $4f^7 5d^0 6s^2$	64 <b>Gd</b> Gadolinium 157.250 $4f^7 5d^1 6s^2$
65 <b>Tb</b> Terbium 158.925 $4f^9 5d^0 6s^2$	66 <b>Dy</b> Dysprosium 162.500 $4f^{10} 5d^0 6s^2$	67 <b>Ho</b> Holmium 164.930 $4f^{11} 5d^0 6s^2$	68 <b>Er</b> Erbium 167.259 $4f^{12} 5d^0 6s^2$	69 <b>Tm</b> Thulium 168.934 $4f^{13} 5d^0 6s^2$	70 <b>Yb</b> Ytterbium 173.055 $4f^{14} 5d^0 6s^2$	71 <b>Lu</b> Lutetium 174.967 $4f^{14} 5d^1 6s^2$	

Fig. 1.4. Rare earth ions and their electronic configurations.

Because of their essential  $4f-4f$  electronic transitions, RE element-embedded luminescent materials are in high demand across a range of applications, including solid-state lasers, illumination, optical fiber amplifiers, and small microchip lasers. Lanthanide elements in the periodic table are called rare earth elements because they occur sporadically in nature. The group of elements known as lanthanides includes from lutetium (Lu,  $Z = 71$ ) to lanthanum (La,

$Z = 57$ ). Although their chemical makeup is identical, their color, optical characteristics, and magnetic properties are different. Because the 4f electrons are protected by the  $5s^2$  and  $5p^6$  orbitals, there is a chemical resemblance. Recent studies draw attention to rare earth ions (also known as Lanthanoids), which could be used as amplifiers and emitters in the IR to Visible spectrum [49-51]. In doped with luminescent glasses, rare earth ions can be subjected to an increase in emission efficiency and enhancing the suitability in solid state lighting applications [28]. There are numerous photonics uses for trivalent RE ions. Neodymium (Nd), erbium (Er), and praseodymium (Pr) ions are well-known for their applications in telecommunications systems. Other elements, besides these RE ions, are the subject of extensive research. Full-color displays use the red, green, and blue light produced by europium (Eu), terbium (Tb), and cerium (Ce). Thulium (Tm) and holmium (Ho) lasers have garnered significant attention in the past decade due to their suitability for a variety of applications. These applications include medicine and eye-safe remote sensing systems, such as laser ranging, coherent Doppler lidar for wind sensing, and wind-shear detection, among others [52].

### ***1.5.1. Characteristics of Rare Earth Ions***

- Unique electronic configuration: The partially occupied 4f orbitals shielded by 5s/5p electrons result in sharp, stable  $f-f$  transitions that are minimally affected by the host environment.
- Narrow spectral lines and hypersensitive transitions: Judd–Ofelt theoretical formulations explain the precise and sensitive nature of the electric dipole transitions, which are critical for laser and photonic devices.
- Influence of local symmetry: Variations in ligand geometry and crystal field strength affect the splitting of multiplet energy levels, leading to hypersensitive transitions and tunable emission properties that serve as sensitive probes of the host matrix.

- High quantum efficiencies and long excited state lifetimes: Doped RE ions exhibit strong luminescence, often enhanced by the absence of nonradiative quenching groups like OH<sup>-</sup>, making them ideal for optical applications [53].
- Catalytic and sensing utility: The reversible redox behavior and strong affinity for ligand coordination allow RE ions to enhance catalytic reactions and selective chemical sensor performance [54].

In complex material applications, rare earth ions are essential due to their unique combination of electrical, optical, structural, and magnetic capabilities. They are excellent candidates for lasers, light-emitting devices, up-conversion phosphors, chemical sensors, and magnetic imaging agents due to their distinct  $4f$  energy levels, restricted emission bandwidths, long luminescence lifetimes, and strong integration into a variety of host matrices. In addition to defining the intrinsic optical transitions of RE ions, the interplay among their electronic structure, local coordination environment, and bonding properties offers numerous ways to adjust their luminescent and magnetic behaviours for a variety of applications.

## 1.6. White Light LEDs

However, luminescent glasses, which are less expensive, more chemically and thermally stable, and devoid of epoxy resin, are set to substitute phosphor in the near future [15]. They are the potential candidate for w-LEDs famed by excellent properties such as easy manufacturing procedure, better transparent materials in the visible region and higher solubility of RE ions (Rare Earth) [18, 24, 25]. These rare-earth-doped luminescent glasses have profound benefits such as good brightness, less energy consumption, higher doping range, and improved chemical and thermal stability as well as modifiable size and shape [12, 23]. Their application varies from lasers, photovoltaics, telecommunications, and wavelength converters to optoelectronic device applications [13, 19, 28].



Commercially acclaimed, an amalgamation of inorganic yellow phosphor ( $\text{Y}_3\text{Al}_5\text{O}_{12}:\text{Ce}^{3+}$ ) with a blue LED chip (InGaN) in the organic epoxy resin. White LEDs based on phosphor conversion require epoxy resin as a binding material between the chip and phosphor interface [13, 18, 20]. These epoxy resins are made up of polymer/organic materials that have many disadvantages due to the constant heat generation leading to depletion of organic resin ultimately resulting in less thermal stability and lower color rendering index, further drawbacks comprising of rapid wear off, low heat dissipation efficiency, and lower transmissivity due to variation in refractive index [23-25].

### ***1.6.1. Methods to Generate White Light***

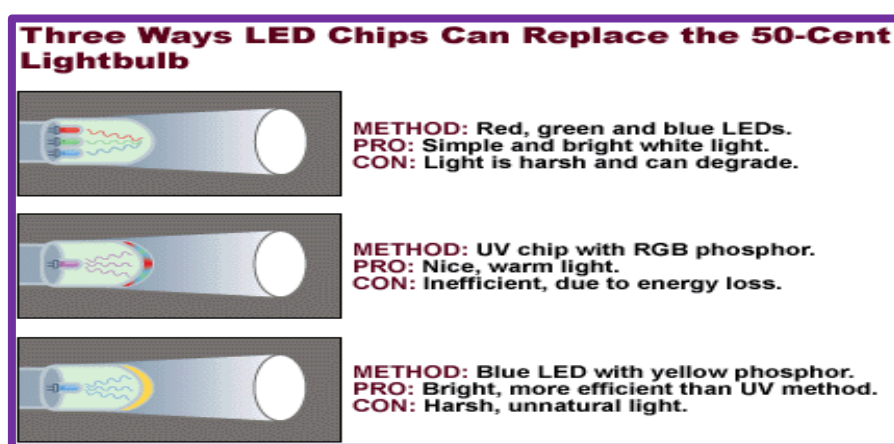


**Fig.1.5.** *Three common ways to generate White light.*

The methods to generate white light in modern lighting applications can be succinctly summarized as follows:

- Multi-chip (RGB) LED combinations
- Blue or near-UV LED-driven phosphor conversion (partial or full)
- Use of transparent glass-ceramic phosphors for stability
- Down-conversion via colloidal quantum dots
- Single-phase white light emitters based on coordination assemblies and MOFs

- Broadband emission from layered halide perovskites based on self-trapped excitons
- Phosphor-free approaches using nanostructured InGaN heterostructures
- Down-conversion using advanced nitride, oxynitride, and fluorosulfide phosphor systems
- Composite approaches such as laser-driven phosphor conversion and phosphor-in-glass/ceramic designs [35, 55].

## Chapter -2: Experimental and Characterization Techniques

---

### 2.1. Selection of Host Materials

Phosphate-based glasses are regarded as a technologically promising candidate for host materials among the various RE (Rare Earth) doped glass matrix (modifiers and formers) because of their properties, which include transparency, low scattering, low viscosity, UV transmittance, isotropic refraction index, and due to laser properties, as well as higher solubility for RE ions [49, 56]. The addition of borate structures provides advantages such as improved chemical durability, increased thermal stability, and an expanded range for adding a significant amount of modifier oxides as compared to pure phosphate as well as pure borate systems [57]. The pure Borate and pure Phosphate glasses can account for their structure for their deficiencies in pure borate glasses, stretching vibration of borates cause high phonon energy ( $1300\text{ cm}^{-1}$ ) resulting in nonradiative relaxation [58] while the hygroscopic nature of pure phosphate causes decreased structural stability than borate glass exhibiting low phonon energy ( $1100\text{ cm}^{-1}$ ) [56]. The benefits of borophosphate glasses have shown results in better ionic conductivities and extended glass forming abilities, optical properties combining than both of pure glass hosts range [12, 59]. Zinc borophosphate glass is utilized in w-LEDs, in semiconductor quantum dots as an excellent dielectric host, and in optoelectronics [60]. In borophosphate glasses, ZnO can be utilized as a glass network modifier by improving chemical durability, enhancing glass stability, and promoting low glass transition temperature, thus advancing the glass matrix in terms of stability in structural and thermal properties [61, 62]. It's non-toxic, accompanied with wide direct band gap as well as huge binding energy, intrinsic emission property and hygroscopic nature makes ZnO suitable for both glass modifier as well as glass former abilities [60]. The  $\text{Na}_2\text{O}$  components ( $\text{Na}^+$  ions) act as intermediate/modifier oxides, stabilizing glass during melting and forming non-bridging oxygen atoms, resulting in the development of a  $\text{BO}_4$

tetrahedral unit and the expansion of borate networks[63]. It can also increase the moisture resistance ability of the borate glass network thus minimizing the hygroscopic nature of the glass [28, 64]. Barium Oxide (BaO) being a heavy metal oxide is utilized to increase the density of the glass to further improve glass structure. BaO has the properties to absorb thermal neutrons and ionizing radiation and provide increased durability in glass structures [65].

## 2.2. Synthesis Procedure

**Melt Quenching Procedure:** In this current work, a set of transparent  $\text{Pr}^{3+}$  doped zinc borophosphate (NBZPBPr) glasses of composition  $(40 - x) \text{B}_2\text{O}_3 + 20 \text{P}_2\text{O}_5 + 15 \text{ZnO} + 15 \text{BaO} + 10 \text{Na}_2\text{O} + x \text{Pr}_6\text{O}_{11}$  were formed via applying melt quenching method. The prepared glasses were labelled as NBZPB, NBZPBPr<sub>0.05</sub>, NBZPBPr<sub>0.1</sub>, NBZPBPr<sub>0.5</sub>, NBZPBPr<sub>1.0</sub> and NBZPBPr<sub>1.5</sub> representing undoped and  $\text{Pr}^{3+}$  embedded concentrations (x) of 0.0, 0.05, 0.1, 0.5, 1.0 and 1.5 mol%, respectively. The raw materials such as boric acid ( $\text{H}_3\text{BO}_3$ , 99.0%), ammonium dihydrogen phosphate ( $\text{NH}_4\text{H}_2\text{PO}_4$ , 99.0%), zinc oxide ( $\text{ZnO}$ , 99.0%), sodium carbonates ( $\text{Na}_2\text{CO}_3$ , 99.0%) and praseodymium (III, IV) oxide ( $\text{Pr}_6\text{O}_{11}$ , 99.99%) were utilized. The raw constituents were weighed as per the stoichiometric proportion and mixed systematically in an agate mortar for an hour using acetone as a wetting agent for a homogeneous smooth blend. Then, the mixture was placed in a container of alumina and heated at 1000 °C for 60 minutes in a programmed electric muffle furnace. The uniform melt was poured onto a preheated brass metal plate and suddenly quenched to form NBZPBPr glass by compressing it with another brass plate. This was further annealed at 300 °C for four hours to reduce internal residue stress and air bubbles formed during the procedure of quenching. The obtained transparent glass samples have been utilized for further characterizations, such as XRD, PL, and TDPL.

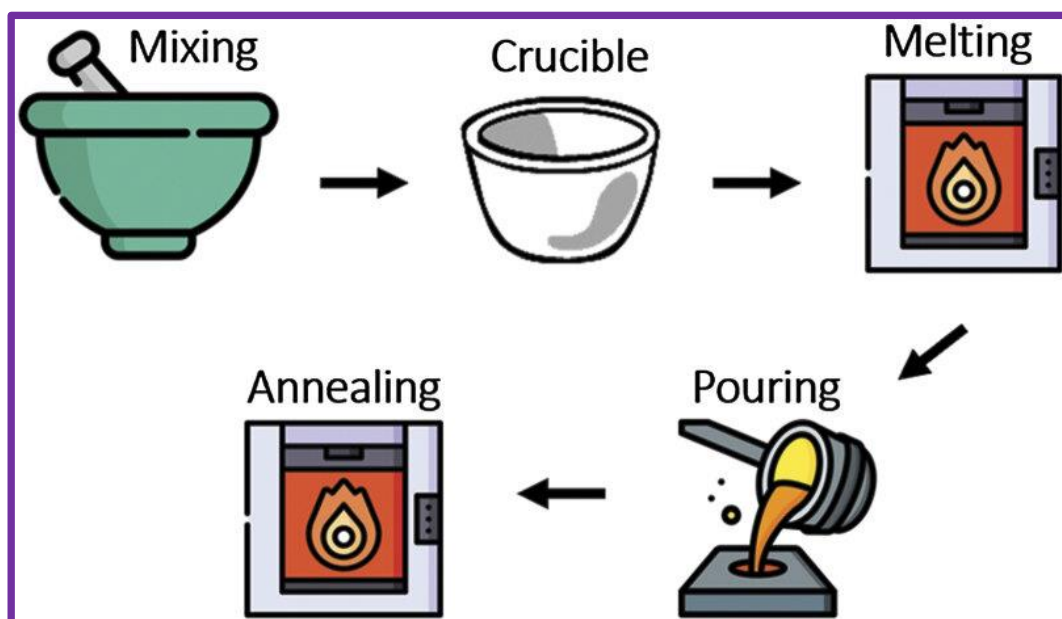


**Fig. 2.1.** *Melt Quenching method Diagram.*

### 2.3. Characterization Techniques

The thermal properties of the NBZPB glass were investigated using DSC measurement with a Setaram Labsys EVO instrument, conducted under an argon atmosphere with a 10°C per minute heating rate from 200 to 1050 °C. The structural characteristics of the NBZPB host and NBZPBPr glasses were observed with a Bruker; D8 advance X-ray diffractometer, which is equipped with a Nickel filter and employs Cu K $\alpha$  ( $\lambda = 1.5406 \text{ \AA}$ ) radiation in the  $2\theta$  scale range of 10° to 70°. Optical absorption analysis of the NBZPBPr glasses was carried out in the wavelength range from the near-UV to the NIR region (350 to 2250 nm) using a Jasco V-770 spectrophotometer. The photoluminescent properties of the NBZPBPr glass samples were investigated using a Shimadzu RF-5301 PC spectrofluorophotometer with a Xenon (150 W) bulb as the excitation source. Additionally, temperature-dependent photoluminescence (TDPL) studies were performed using an Ocean Optics (FLAME-S-XR1-ES) spectrophotometer.

### ***2.3.1. Thermal Analysis***

Differential scanning calorimetry and thermogravimetric analysis are two examples of thermal analysis techniques that use controlled heating or cooling of materials to measure changes in temperature, heat flow, weight, or other characteristics. This is helpful in determining the rates of breakdown, phase transitions, thermal behavior, and thermal stability of a material. DSC is a thermal analysis procedure that assesses the movement of heat into or out of a sample as a function of temperature or time. When a sample is chilled or heated, it provides details about the physical and the chemical reactions occurring within it. In DSC, a sample and the fixed reference material are heated or cooled to the same temperature. By comparing the heat flow between the sample and the reference, which logs any variations, phase shifts, melting temperatures, crystallization, and other thermal events can all be identified. Melting points, phase transitions, thermal stability, decomposition kinetics, glass transition analysis, and crystallinity can all be determined using DSC.

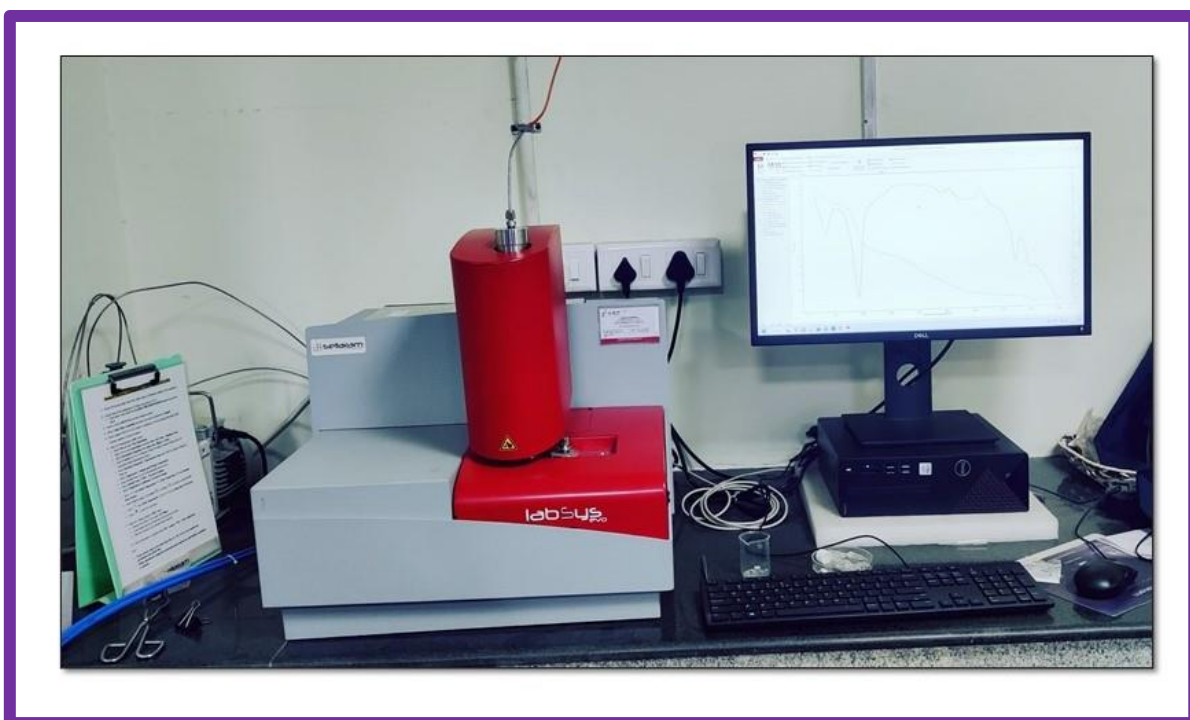


**Fig. 2.2.** *The Setaram Labsys Evo instrument.*

Weight variations in samples that are heated or cooled under exact temperature control can be analyzed using TGA. It provides information about the materials' composition, deterioration, and thermal stability. In TGA, a sample is heated or cooled while being continuously weighed at a constant speed. Weight gain or loss is monitored as a function of temperature or time, indicating thermal phenomena like breakdown, oxidation, desorption, or changes in moisture content. TGA is helpful for analyzing breakdown and weight loss, as well as determining heat stability and degradation kinetics. The DSC TGA was performed by using the Sataram Labsys Evo instrument.

### 2.3.2. X-ray diffraction (XRD)

X-ray diffraction analysis is a method of defining the arrangement of atoms within a crystal. X-ray diffraction analysis (XRD) involves exposing the substance to incoming X-rays and examining the intensity and scattering trajectory of the radiation.

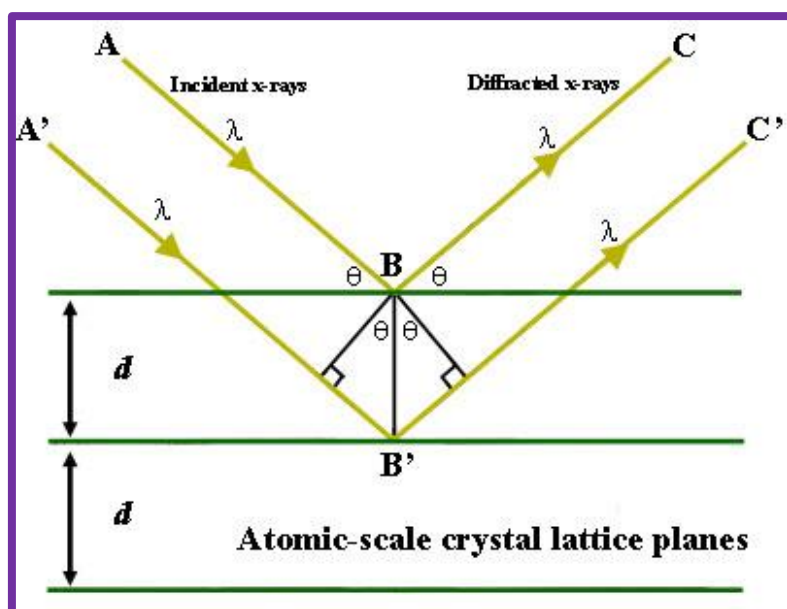


Fig. 2.3. Bragg's Diagram.

The length between lattice planes in crystalline materials and the X-ray wavelengths are of comparable magnitude. The atoms' surrounding electron clusters will distribute the X-rays

when they enter the substance. The X-rays' constructive interference is caused by the periodicity of planes within the lattice, and a plot of the intensity of the scattered X-rays versus angle  $2\theta$  shows Bragg's law. Bragg's law as shown by the equation

$$n\lambda = 2d \sin \theta \quad (2.1)$$

here  $n$  depicts the integer,  $\lambda$  is the wavelength of the X-rays,  $d$  is the interplanar spacing causing the diffraction, and  $\theta$  is the diffraction angle [66].

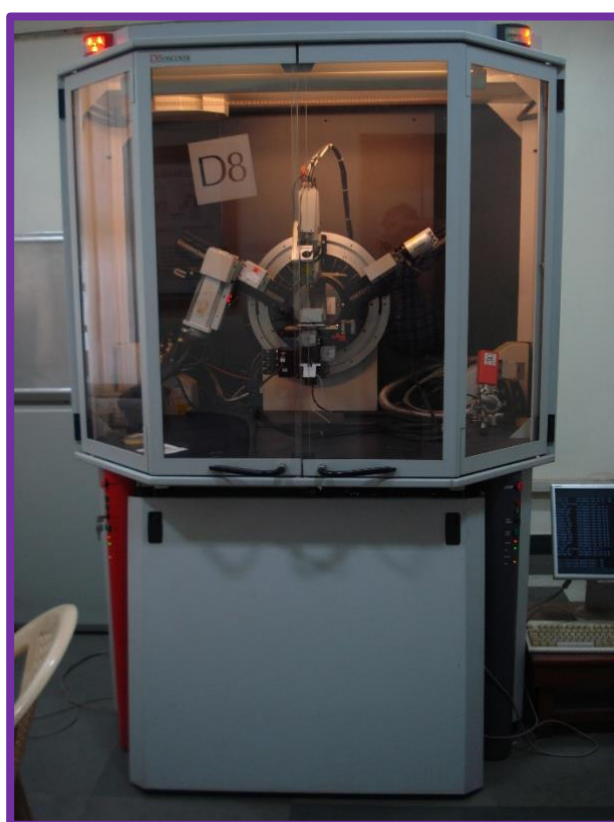


**Fig.2.4.** *High-resolution X-ray diffractometer.*

### ***2.3.3. Fourier Transform Infrared (FT-IR) Spectroscopy***

Fourier transform infrared spectroscopy is a highly versatile, rapid, and non-destructive analytical technique that has become indispensable in numerous scientific and industrial fields. Its fundamental principle—measuring the absorption of IR radiation corresponding to



molecular vibrational transitions—enables the generation of unique spectral fingerprints that are critical for qualitative and quantitative analyses.

The technique takes advantage of the quantized vibrational energy levels present in all molecules. These vibrational modes produce distinctive absorption bands when they are stimulated by infrared (IR) radiation. These bands can be carefully categorized into spectral regions to enable qualitative and quantitative analysis for a variety of applications.

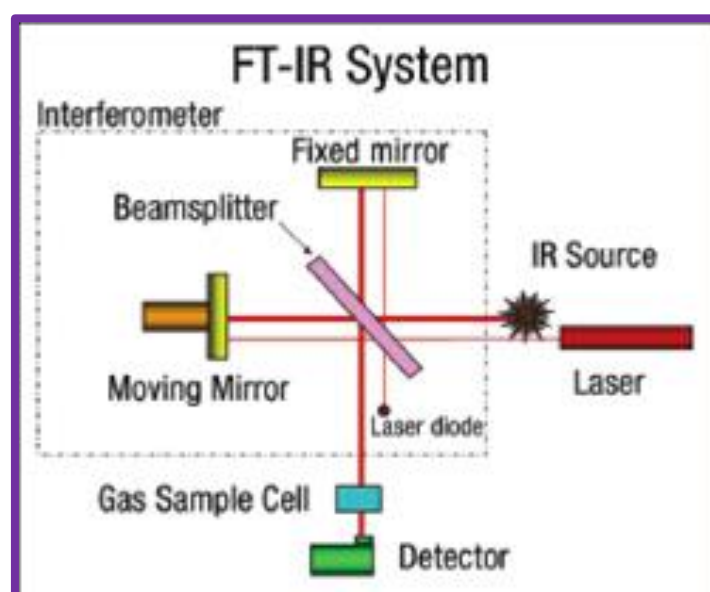


**Fig.2.5.** *Schematic Working Diagram of FT-IR.*

Fourier Transform Infrared (FTIR) spectroscopy operates by transmitting a broadband source of infrared radiation through a sample, wherein specific frequencies are absorbed due to molecular vibrational transitions. The resultant signal, known as an interferogram, is converted into a spectrum through Fourier transformation. The x-axis of the FTIR spectrum is typically represented in wavenumbers ( $\text{cm}^{-1}$ ), which are directly proportional to vibrational frequency and inversely proportional to wavelength. Each absorption band observed in the spectrum corresponds to a distinct vibrational mode of molecular bonds—such as stretching, bending, twisting, or rocking. These characteristic vibrational frequencies are influenced by bond type,

atomic mass, and molecular environment, thereby enabling the identification of functional groups and providing a unique spectral "fingerprint" for molecular identification [67].

FTIR instruments are typically equipped with an interferometer, a broadband IR source, detectors capable of rapid data acquisition, and computer algorithms that execute the Fourier transform.

FTIR Spectral Regions:

1. High Wavenumber Region (Approximately 4000–2500  $\text{cm}^{-1}$ )
2. Mid Wavenumber Region (Approximately 2500–1500  $\text{cm}^{-1}$ )
3. Fingerprint Region (Approximately 1500–400  $\text{cm}^{-1}$ )

#### ***2.3.4. Optical Absorption Spectral Analysis***

Measurements of the samples' transmission, reflectance, and absorption of light were made using a UV/VIS/NIR spectrophotometer. A light source that generates light in the UV to NIR (200 to 1500 nm) range affects the sample in spectroscopy, and the light that is transmitted is captured at the sample's other end. The light that was supplied includes the optical data of the sample after it has interacted with them. In UV-VIS spectroscopy, this method is used to measure the optical studies of various organic and inorganic materials [68].

UV/VIS spectrum makes use of the Beer-Lambert equation. The Beer-Lambert equation states that the amount of radiation striking an absorbing solution and the solution's concentration both affect how quickly the intensity of the radiation drops as the thickness of the solution is changed. The mathematical equation for absorbance ( $A$ ) is mentioned as:

$$A = \log_{10} (I_t/I_0) \quad (2.2)$$

where,  $I_0$  and  $I_t$  denotes the incident light intensity and transmitted light intensity, respectively.

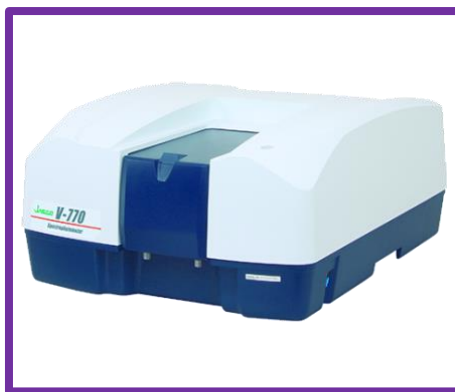


**Fig.2.6.** *V-770 UV-Visible/NIR Spectrophotometer up to 3200 nm.*

In a UV/VIS/NIR spectrophotometer, a converged beam from the light source enters the monochromator. The matching UV and NIR light sources were deuterium and tungsten lamps. The light is scattered by the monochromator's grating and leaves through the exit slit. Using a sector mirror, this light is split into two streams, one of which strikes the reference sample (like solvent) and the other the sample being measured. The light from the sample or reference sample passes through the detector and is incident upon it. A detector photomultiplier tube is used to record the spectrum. After that, software was utilized to examine the recorded spectrum and create a wavelength-scale spectrum.

### ***2.3.5. Photoluminescence (PL) Spectroscopy***

Photoluminescence (PL) spectroscopy is an optical characterization technique that provides detailed insight into the electronic and optical properties of semiconductor and nanostructured materials by analyzing the light emitted from a sample after it absorbs photons from an external excitation source [69]. When the sample is exposed to light whose photon energy surpasses the material's band gap, electrons are excited from the valence band to the conduction band. This results in non-equilibrium electron-hole pairs that eventually recombine radiatively, emitting photons with energies and intensities typical of the material's intrinsic properties and defect states. This is the fundamental physical principle underlying photoluminescence (PL).



**Fig.2.7.** *Shimadzu RF-5301 PC spectrofluorophotometer with a Xenon (150 W) bulb.*

In a typical PL spectrometer procedure, the experimental set-up is centered around a well-organized optical system that comprises several critical components: an excitation source, collection optics, a wavelength dispersion unit (generally a monochromator or spectrograph), and a sensitive detector such as a charge-coupled device (CCD) or a photomultiplier tube (PMT) [70].

The applications of PL spectroscopy in luminescent glasses extend beyond academic research; they are integral to the development of modern lighting, display technologies, and photovoltaic devices. In white LED technology and phosphor-in-glass systems, accurately characterizing the emission properties leads to improved color rendering, higher efficiency, and longer operational lifetimes [71]. In the field of materials research, PL spectroscopy is a strong and adaptable instrument, especially for the identification and description of luminous glasses. Emission spectra, decay kinetics, and the interactions between luminescent centers and the glass host may all be thoroughly examined because to its non-destructive nature and excellent time-resolved and steady-state measuring capabilities. Our basic knowledge of these materials is improved by the insights gained by PL spectroscopy, which also drives the creation of next-generation optical devices including LEDs, solar concentrators, and display technologies [72].

### ***2.3.6. Temperature Dependent PL Spectroscopy (TDPL)***

Temperature dependent photoluminescence (PL) spectroscopy for luminescent glass is an optical characterization technique that measures the changes in the luminescence properties—such as emission intensity, spectral shape, and sometimes lifetime—as a function of temperature [73]. Non-contact optical thermometry is one of the main uses for this temperature-sensitive technique. Utilizing variations in the photoluminescent emission when the lattice environment of a semiconductor or insulator is thermally changed, temperature-dependent PL spectroscopy can influence energy band structures and carrier recombination processes. By capturing PL spectra throughout a broad temperature range, variations in the bandgap energy, excitonic binding, and even trion production may be objectively investigated.

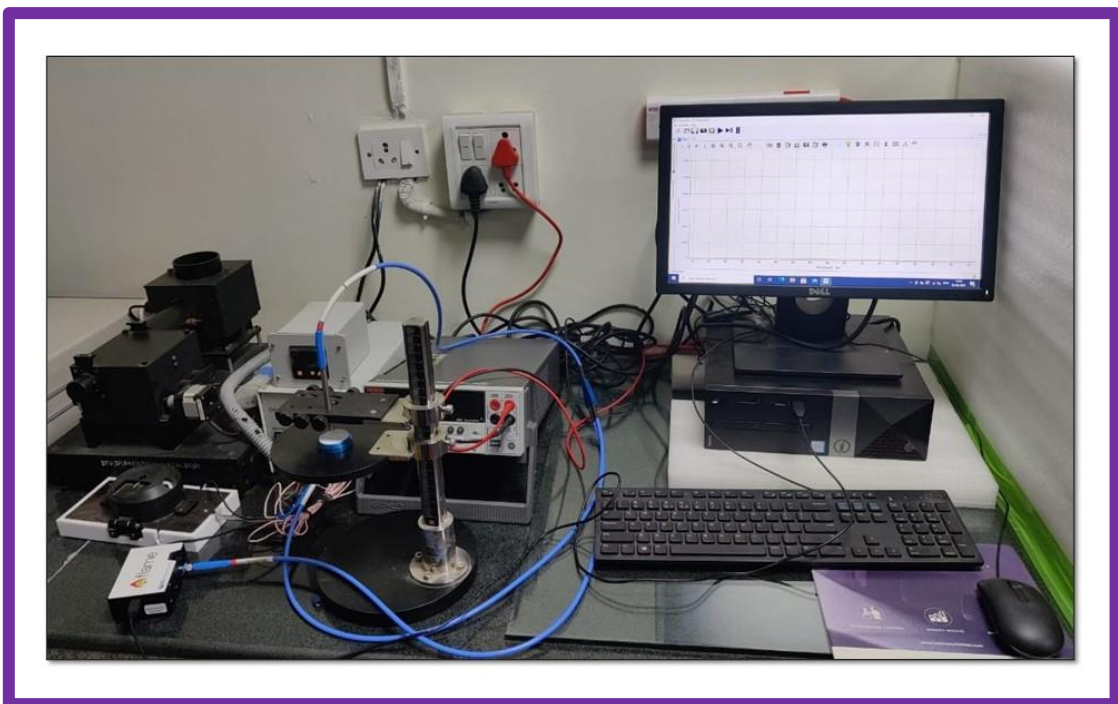


**Fig. 2.8.** *Ocean Optics (FLAME-S-XR1-ES) Spectrophotometer*

The photoluminescence (PL) process is fundamentally governed by the radiative recombination of photoexcited electron-hole pairs and is significantly influenced by temperature-dependent phenomena. As the temperature increases, lattice expansion and

elevated phonon populations enhance electron–phonon interactions, which in turn promote nonradiative recombination pathways, resulting in a reduction of PL intensity. Additionally, the semiconductor bandgap typically exhibits a narrowing trend with increasing temperature, a behavior attributed to both thermal lattice expansion and the temperature sensitivity of electron–phonon coupling. This temperature-induced bandgap variation is commonly described by the Varshni equation, which provides an empirical relationship between bandgap energy and temperature. Temperature-dependent PL spectroscopy is also extensively used to characterize phosphors intended for high-power light–emitting diode (LED) applications. Detailed temperature-dependent studies reveal that the thermal quenching behavior, Stokes shifts, and lifetimes of these emissions vary with the host crystal field strength and electron–phonon coupling.

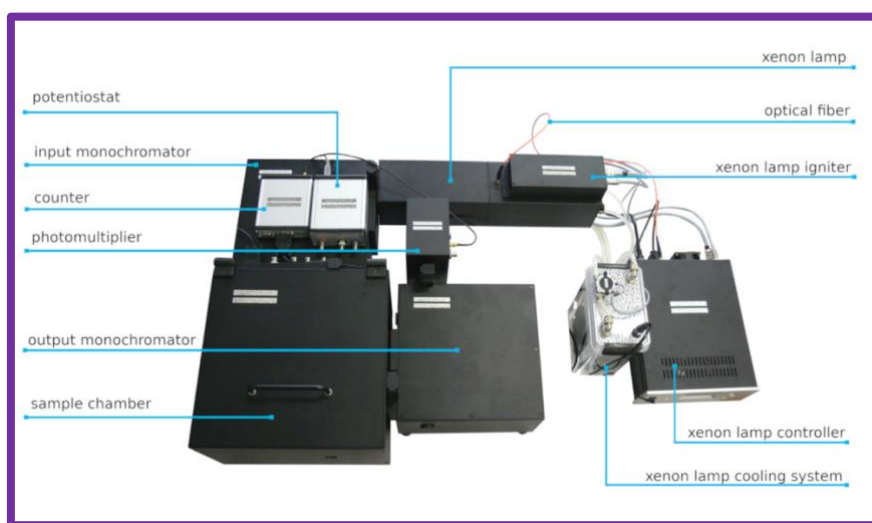


**Fig. 2.9.** *Labelled Diagram of TD-PL Spectrofluorometer*

The temperature-dependent PL spectrometer working principle comprises the following key aspects:

- An excitation module that delivers fixed or pulsed wavelengths to reliably generate excitons and electron–hole pairs;

- An optical collection system that filters and spatially resolves the emitted light;
- Temperature control systems that enable measurements under stable and precisely varied thermal conditions, ensuring that the sample reaches equilibrium before data acquisition;
- Spectral and time-resolved detection that together provide comprehensive datasets characterizing the emission intensity, spectral positions, linewidths, and decay kinetics; and
- Data analysis frameworks that extract underlying physical parameters from the temperature-induced changes in the PL features.

These elements work together and seamlessly integrate to help researchers understand how temperature affects PL processes. This enables them to assess and improve material qualities for cutting-edge optoelectronic applications [74, 75].

## Chapter 3: Results and Discussion

### 3.1. Thermal Analysis

The thermal features of the NBZPB glass have been estimated with the help of DSC analysis [76]. DSC is a thermo-analytical method that precisely quantifies the difference in heat required to upsurge the sample temperature compared to that of a standard reference sample, as a function of temperature. Fig. 3.1 illustrates the DSC thermo-graph for the NBZPB host glass was captured with a 10 °C/min heating rate in the argon atmosphere, covering temperature profiles from 200 to 1050 °C. The DSC graph depicts two types of transitions, one being endothermic and the other being exothermic.

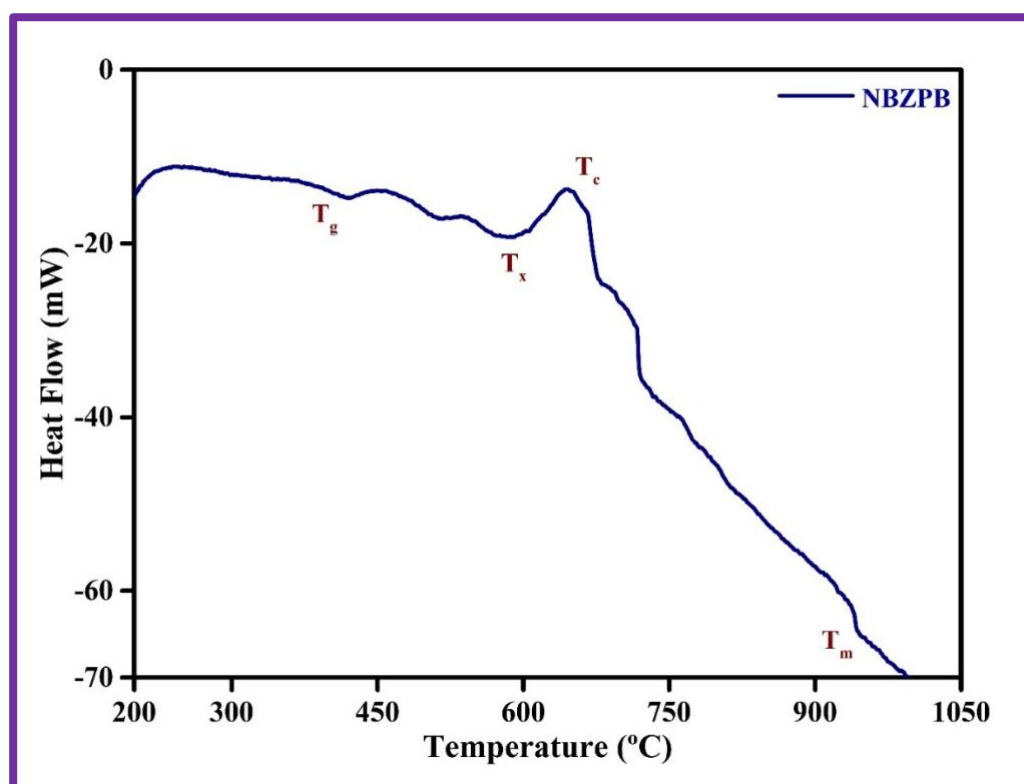


**Fig. 3.1.** Differential scanning calorimetry (DSC) for the NBZPB glass host.



From Fig. 3.1, the graph exhibits numerous temperature characteristics identified as the specific glass transition temperature ( $T_g = 385\text{ }^{\circ}\text{C}$ ), onset crystallization temperature ( $T_x = 489\text{ }^{\circ}\text{C}$ ), peak crystallization temperature ( $T_c = 645\text{ }^{\circ}\text{C}$ ) and melting temperature ( $T_m = 947\text{ }^{\circ}\text{C}$ ), respectively. The thermal stability ( $\Delta T$ ) factor for the NBZPB host glass was computed using the following equation [49, 77]:

$$\Delta T = T_x - T_g \quad (3.1)$$

A higher  $\Delta T$  factor value indicates greater stability of the glass host. According to the literature, a  $\Delta T$  value exceeding  $100\text{ }^{\circ}\text{C}$  is considered to be indicative of more thermal stability. In this study, the computed  $\Delta T$  factor was obtained to be  $104\text{ }^{\circ}\text{C}$ , surpassing  $100\text{ }^{\circ}\text{C}$ , which is higher than values reported for other glass matrices in the literature [49]. Therefore, these findings suggest that the NBZPB host glass exhibits excellent thermal stability, making it well-suited for optoelectronic applications.

### 3.2. Structural and Vibrational Analysis

The diffraction profiles for the formed NBZPB and NBZPBPr<sub>0.1</sub> glasses are shown in Fig. 3.2, with a  $2\theta$  range from  $10^{\circ}$  to  $70^{\circ}$ .

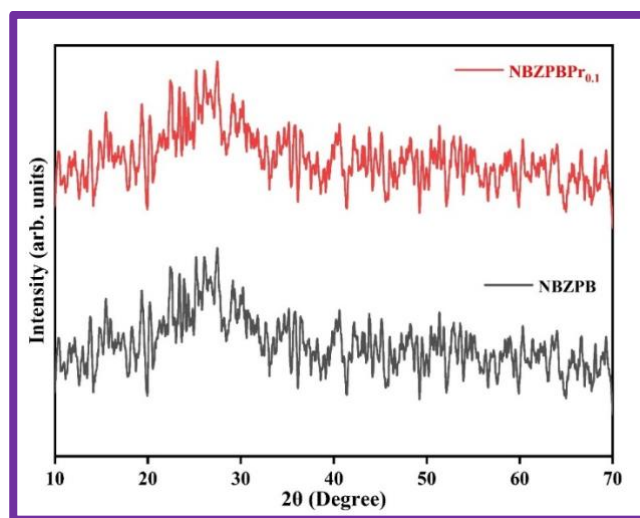


**Fig. 3.2.** X-ray diffraction (XRD) profiles for the NBZPB host and NBZPBPr<sub>0.1</sub> glasses.

The XRD profiles display a broad hump between 20 ° and 40 ° with no distinct Bragg's peaks, confirming the absence of crystalline structure in the glass. Moreover, the inclusion of the dopant  $\text{RE}^{3+}$  ( $\text{Pr}^{3+}$ ) ions into the NBZPB host does not affect its non-crystalline nature. Thus, the diffraction profiles affirm the amorphous or glassy nature of the NBZPBPr glass samples. Fourier transform infrared (FT-IR) spectroscopy is an essential tool for categorizing various functional linkages and structural bonds in the glass matrix.

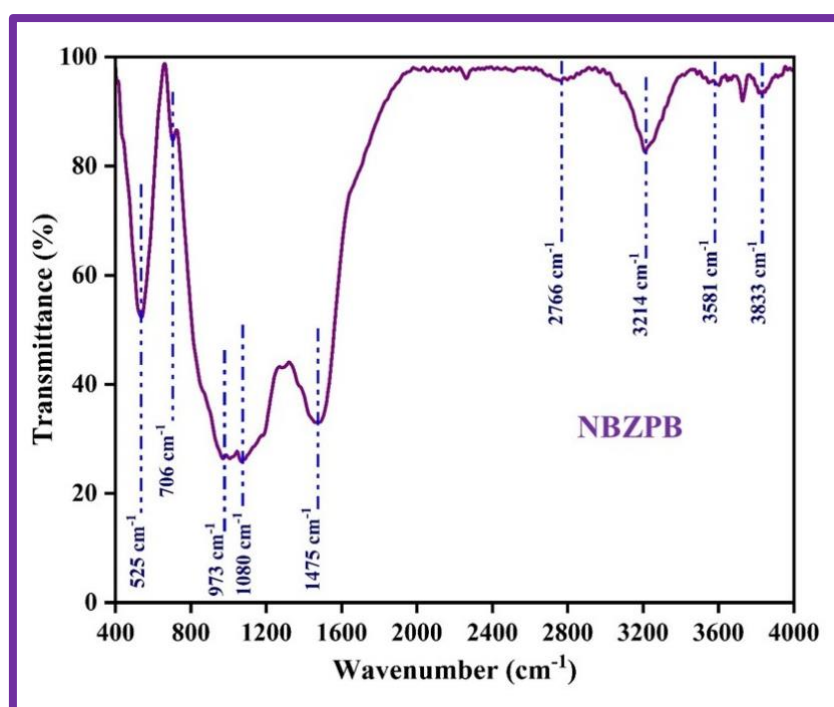


**Fig. 3.3.** *FT-IR spectrum for the NBZPB host glass.*

Fig. 3.3 depicts the FT-IR spectrum of the NBZPB glass composition that has been captured at ambient temperature within the wavenumber range of 400 to 4000  $\text{cm}^{-1}$ . The spectrum of the NBZPB host glass features several vibrational shoulders at 525, 706, 973, 1080, 1475, 2766, 3214, 3581 and 3833  $\text{cm}^{-1}$ . The shoulder around 525  $\text{cm}^{-1}$  likely corresponds to the vibration of the Zn-O bond in the  $\text{ZnO}_4$  structure, as well as the harmonic of symmetric P-O-P bending vibrations [78, 79]. The vibrational band observed at 706  $\text{cm}^{-1}$  is linked to the B-O-B linkage in borate networks, encompassing both the B-O bond and the overlapping vibrations of the

bridging oxygen atoms, which interact with the symmetric stretching of the bridging oxygen ions in P-O-P vibration [80-84]. The band positioned at  $973\text{ cm}^{-1}$  is associated with the B-O bond stretching of the  $\text{BO}_4$  tetrahedral borons structures [81]. The band located around at wavenumber  $1080\text{ cm}^{-1}$  may be associated with the asymmetric stretching of the P-O-P linkage [86, 87]. The asymmetric stretching vibration of trigonal  $\text{BO}_3$  structures may be attributed to the peak at  $1475\text{ cm}^{-1}$  [81, 87, 88]. The shoulder peak at  $2766\text{ cm}^{-1}$  can be associated with the presence of the -OH group and hydrogen bonding [89], while the shoulder peaks at  $3581$  and  $3833\text{ cm}^{-1}$  are associated with the stretching vibration of the hydroxyl group [81, 90].

### 3.3. Optical Absorption Spectral Analysis

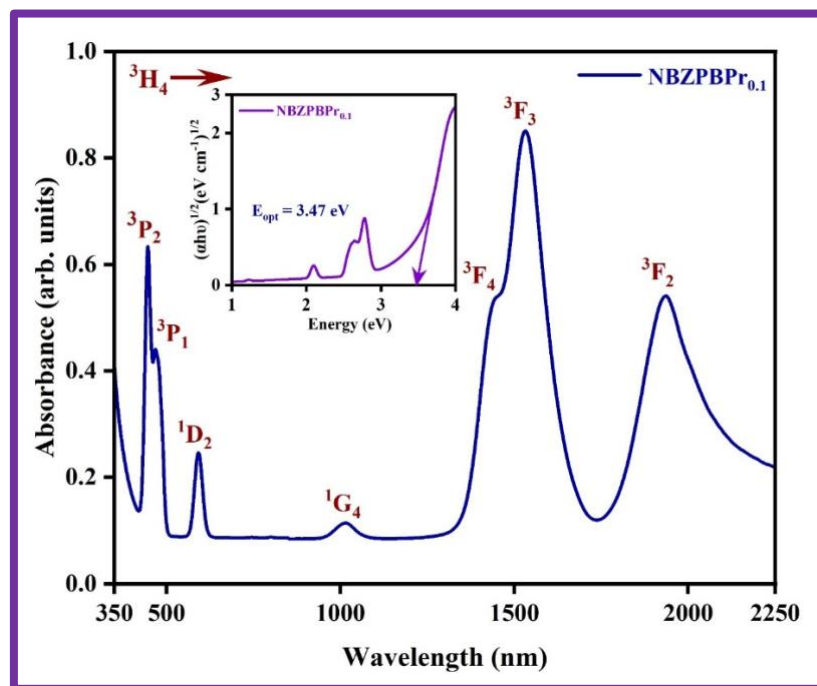


**Fig. 3.4.** Optical absorption spectrum of 0.1 mol%  $\text{Pr}^{3+}$  doped NBZPB glass sample in the n-UV-VIS-NIR region. [Inset signifies the indirect allowed band gap energy of the NBZPBPr<sub>0.1</sub> glass sample using Tauc's plot].

Fig. 3.4 presents the room temperature optical absorption spectrum for the NBZPBPr<sub>0.1</sub> glass captured within the specific wavelength range of 350 to 2250 nm. The spectrum displays seven

distinct absorption peaks at 446, 467, 592, 1014, 1443, 1534, and 1936 nm. The absorption peaks in the blue region (446 & 467 nm) correspond to the transitions from the ground level ( $^3H_4$ ) to excited levels such as  $^3P_2$ , &  $^3P_1$ . The single absorption peak in the visible region (592 nm) is attributed to the  $^3H_4 \rightarrow ^1D_2$  transition, while four peaks in the NIR region (1014, 1443, 1534 & 1936 nm) are linked to the transitions from the ground level ( $^3H_4$ ) to different excited levels such as  $^1G_4$ ,  $^3F_4$ ,  $^3F_3$ , and  $^3F_2$ , respectively. The assignment and determination of these absorption peaks are based on the following procedure specified in the literature by Carnell et al. [91]. Among these peaks, the bands at 446 and 1534 nm, corresponding to the  $^3H_4 \rightarrow ^3P_2$  and  $^3H_4 \rightarrow ^3F_3$  transitions are notably more intense than the others and considered as hypersensitive transitions [19, 49]. Hypersensitive transitions are highly influenced by the local environment of  $Pr^{3+}$  ions in the glass host matrix. To understand the bonding character in the prepared NBZPBPr glasses, the nephelauxetic ratio ( $\bar{\beta}$ ) and bonding parameter ( $\delta$ ) were computed using the standard formulas available in the literature [92]. The estimated  $\bar{\beta}$  value for the NBZPBPr<sub>0.1</sub> glass was found to be 0.996. Additionally, the  $\delta$  value for the NBZPBPr<sub>0.1</sub> glass was calculated to be 0.270. The bonding parameters can be either negative or positive depending on whether the ligand field around the  $RE^{3+}$  ion exhibits ionic or covalent bonding. Based on the findings, the positive estimated value of  $\delta$  indicates that the bonding character in the prepared glasses is predominantly covalent.

In non-crystalline materials, the energy band gap is the energy range amid the conduction band and valence band. The optical band gap ( $E_{opt}$ ) refers to the energy required for a photon to be absorbed by the material [93]. The visible absorption edge in the UV range is often used to examine energy bands and optical transitions in both amorphous and crystalline materials. Davis and Mott's approach was used to evaluate the  $E_{opt}$  for the prepared NBZPBPr glass based on the absorption spectral data [19]:

$$(\alpha h\nu) = C(h\nu - E_{opt})^q \quad (3.2)$$

In equation (3.2),  $\alpha$  implies the absorption coefficient,  $C$  symbolizes the constant related to the band tailing parameter,  $h$  is Planck's constant,  $E_{opt}$  signifies the optical band energy values and  $\nu$  represents the frequency of radiation, respectively. The parameter  $q$  depends on the kind of transition and is assigned as 3 (for indirect forbidden), 1/3 (for direct forbidden), 2 (for indirect allowed) and 1/2 (for direct allowed) transitions, respectively. The  $E_{opt}$  values for indirect allowed transitions were computed by Tauc's graph by extrapolating the straight-line region of the diagram among the  $(\alpha h\nu)^{1/2}$  vs energy ( $h\nu$ ) and are shown in the inset of Fig. 3.4. The estimated  $E_{opt}$  values for an indirect allowed transition of the prepared NBZPBPr<sub>0.1</sub> glass is 3.47 eV. Moreover, another parameter i.e., refractive index ( $n$ ) can be assessed with the help of the Dimitrov et al. relation [2, 46] :

$$\frac{n^2-1}{n^2+2} = 1 - \sqrt{\frac{E_{opt}}{20}} \quad (3.3)$$

The evaluated value of the refractive index ( $n$ ) for NBZPBPr is 2.27.

### 3.4. Luminescent Studies

To comprehend the emission profiles of the formed NBZPBPr glasses, it is very much essential to recognize the excitation wavelengths of Pr<sup>3+</sup> ions. Due to this reason, the ambient temperature excitation spectrum of 0.1 mol% Pr<sup>3+</sup> embedded NBZPB glass (NBZPBPr<sub>0.1</sub>) has been gauged in the range of 400 to 525 nm via pumping the emission wavelength at 602 nm and is presented in Fig. 3.5. The excitation spectrum consists of three intense peaks in the blue region, such as 446, 467 and 484 nm corresponding to the transitions <sup>3</sup>H<sub>4</sub> → <sup>3</sup>P<sub>2</sub>, <sup>3</sup>H<sub>4</sub> → <sup>3</sup>P<sub>1</sub> and <sup>3</sup>H<sub>4</sub> → <sup>3</sup>P<sub>0</sub> of the Pr<sup>3+</sup> ions [49, 95]. For all three peaks, the excitation peak around 446 nm (<sup>3</sup>H<sub>4</sub> → <sup>3</sup>P<sub>2</sub>) shows the highest intensity as compared to the other two remaining peaks. Henceforth,

the peak at 446 nm ( $^3H_4 \rightarrow ^3P_2$ ) has been selected as the excitation wavelength to measure the emission profiles of the series of prepared NBZPBPr glasses.

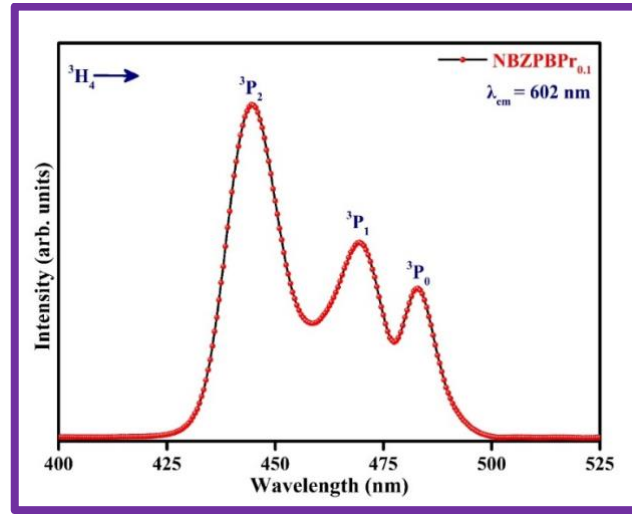


**Fig. 3.5.** PLE spectrum for the NBZPBPr<sub>0.1</sub> glass with fixed 602 nm emission wavelength.

The emission profiles for the prepared NBZPBPr glasses are exhibited in Fig. 3.6. The emission profiles have been captured in 525 to 725 nm at an intense blue excitation wavelength of 446 nm.

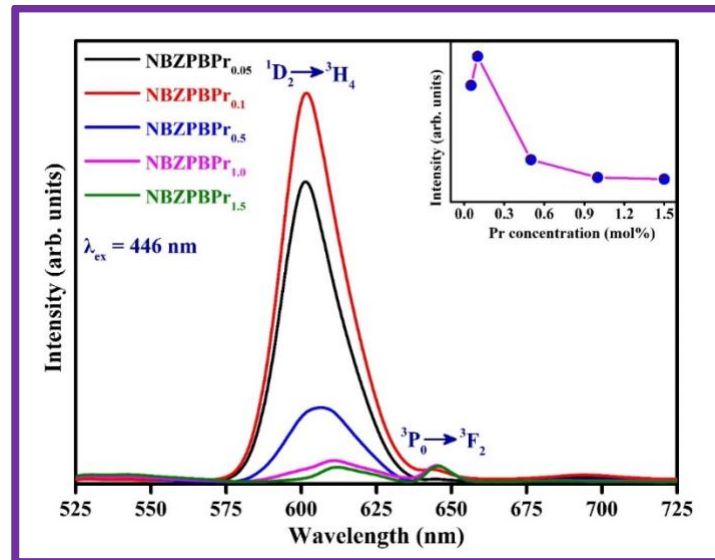


**Fig. 3.6.** PL spectra for the Pr<sup>3+</sup> doped NBZPBPr glass samples for excitation at  $\lambda_{ex} = 446$  nm.

The inset plot shows the variation of PL intensity of the emission peak ( $^1D_2 \rightarrow ^3H_4$ ) with varying Pr<sup>3+</sup> concentration ions in NBZPB glasses.

From Fig. 3.6, it has been noted that the emission profiles consist of two peaks in the visible region at 602 and 646 nm associated with the  $^1D_2 \rightarrow ^3H_4$ ,  $^3P_0 \rightarrow ^3F_2$  transitions of  $Pr^{3+}$  ions [76, 95, 96]. The emission peak at 602 nm ( $^1D_2 \rightarrow ^3H_4$ ) observed in the orange-red region of the electromagnetic spectrum exhibits the highest intensity among all emission peaks. The emission peak intensity ( $^1D_2 \rightarrow ^3H_4$ ) increases along with increasing the doping concentration of  $Pr^{3+}$  ions from 0.05 to 0.1 mol% beyond that the emission intensity decreases with increasing the doping concentration of  $Pr^{3+}$  ions up to 1.5 mol%. This occurs due to the concentration quenching mechanism. As seen in the inset of Fig. 3.6, the correlation between the emission intensity variation of  $^1D_2 \rightarrow ^3H_4$  peak and dopant ( $Pr^{3+}$ ) ion contents. As the content of dopant ions rises, the average distance amid  $Pr^{3+}$ - $Pr^{3+}$  ions diminishes in the host matrix. Consequently, non-radiative energy transfer occurs among dopant ions through cross-relaxation channels, which leads to concentration quenching. Fig. 3.6 illustrates that as the doping concentration of  $Pr^{3+}$  ion increases, a significant red shift is observed for the  $^1D_2 \rightarrow ^3H_4$  emission transition. The peak wavelength of the  $^1D_2 \rightarrow ^3H_4$  transition in NBZPBPr glasses ranges from 601 to 612 nm for  $Pr^{3+}$  ion concentrations of 0.05 to 1.5 mol%, indicating a red shift in this peak. This peak may relate to the site distribution of  $Pr^{3+}$  ions in the vicinity of ligand fields [49]. Fig. 7 illustrates the energy level scheme, highlighting key processes such as excitation, emission and other transition mechanisms, including non-radiative and cross-relaxation pathways. Upon illumination of the NBZPBPr glass, the  $Pr^{3+}$  ions are excited from the ground state ( $^3H_4$ ) to the excited state ( $^3P_2$ ). The ions in the excited state ( $^3P_2$ ) then undergo non-radiative relaxation, resulting in the emission from the metastable level ( $^1D_2$ ). As a result, NBZPBPr glasses emit visible light at wavelengths of 602 nm ( $^1D_2 \rightarrow ^3H_4$ ) and 646 nm ( $^3P_0 \rightarrow ^3F_2$ ), respectively. The potential cross-relaxation pathways are given below and depicted in Fig. 3.7 [32].

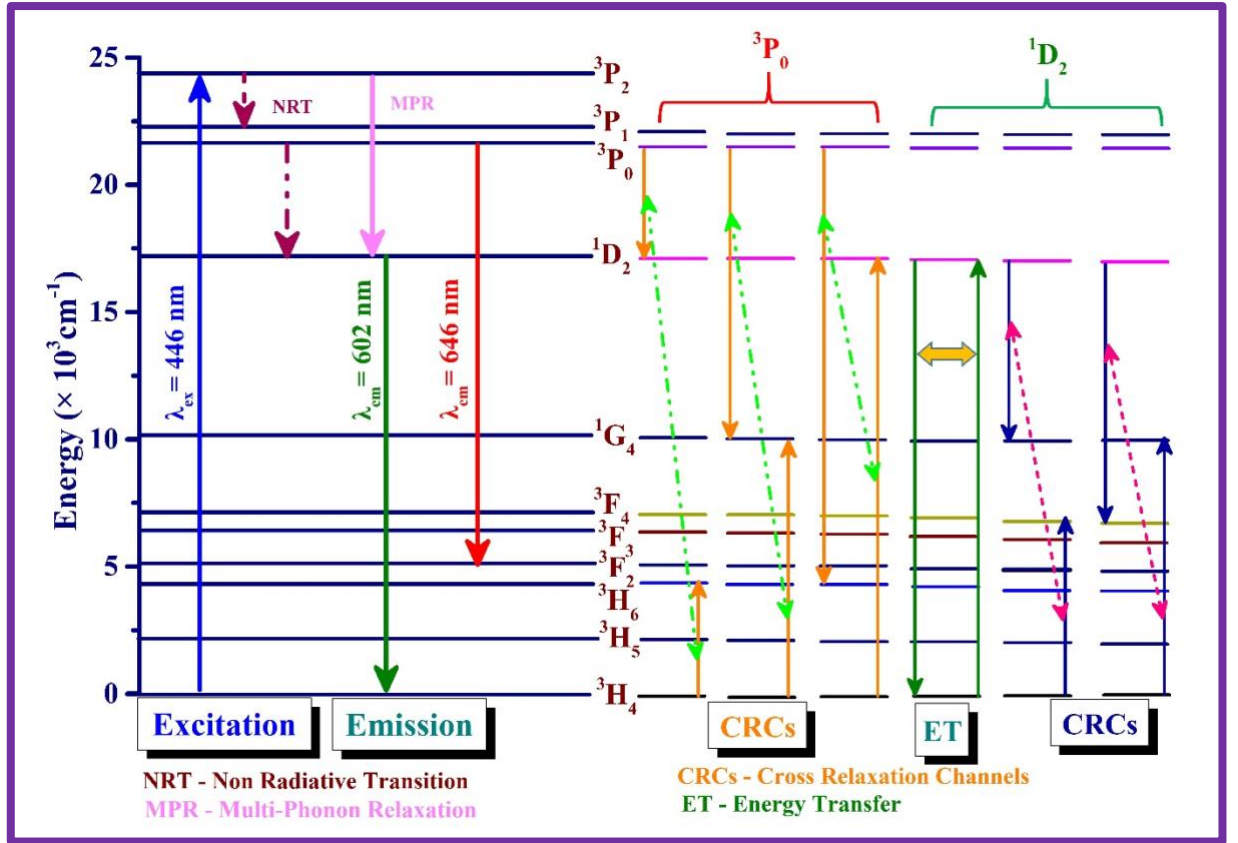


**Fig. 3.7.** Partial Energy level scheme for the  $\text{Pr}^{3+}$  doped NBZPB glass samples.

$$\text{CRC01: } ({}^3\text{P}_0 + {}^1\text{D}_2) \rightarrow ({}^3\text{H}_4 + {}^3\text{H}_6)$$

$$\text{CRC02: } ({}^3\text{P}_0 + {}^1\text{G}_4) \rightarrow ({}^3\text{H}_4 + {}^1\text{G}_4)$$

$$\text{CRC03: } ({}^3\text{P}_0 + {}^3\text{H}_6) \rightarrow ({}^3\text{H}_4 + {}^1\text{D}_2)$$

$$\text{CRC04: } ({}^1\text{D}_2 + {}^1\text{G}_4) \rightarrow ({}^3\text{H}_4 + {}^3\text{F}_4)$$

$$\text{CRC05: } ({}^1\text{D}_2 + {}^3\text{F}_4) \rightarrow ({}^3\text{H}_4 + {}^1\text{G}_4)$$



### 3.5. Evaluation of CIE coordinates, Correlated Color Temperature (CCT) and Color Purity

The evaluation and quantification of a color emitted through the material are shown as colorimetry. Commission Internationale de l'Eclairage (CIE) coordinates are crucial for determining the color of emitted light through synthesized materials under appropriate excitation. Chromaticity coordinates were derived from the emission profiles of the NBZPBPr glasses following established procedures in the literature [13]. Under blue excitation, the color ( $x, y$ ) coordinates (0.602, 0.390) for the optimized NBZPBPr<sub>0.1</sub> glass have been located in the orange-red area of the CIE graph and presented in Fig. 3.8.

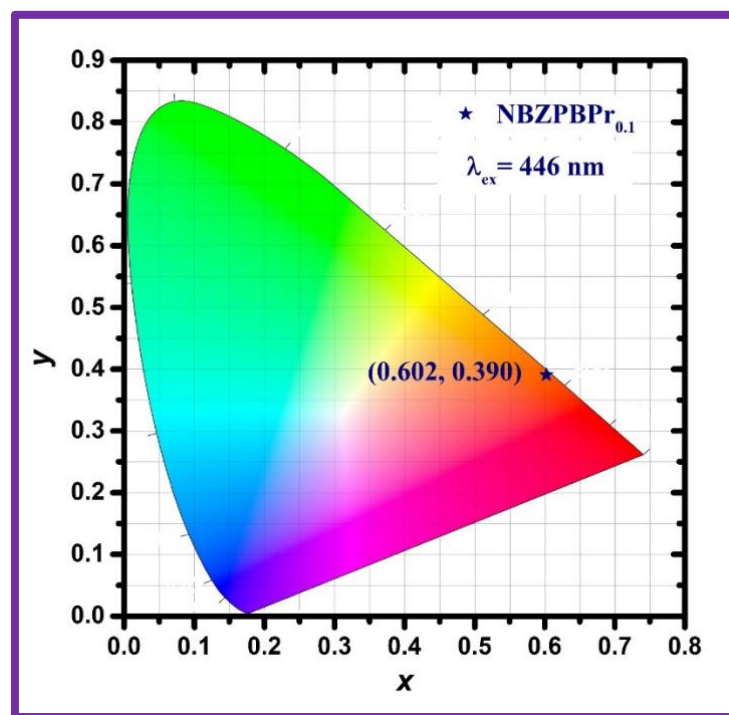


**Fig. 3.8.** CIE chromaticity Plot of the NBZPBPr<sub>0.1</sub> glass under 446 nm excitation wavelength.

Moreover, the correlated color temperature (CCT) of the prepared NBZPBPr glasses were measured via applying the McCamy theoretical relation [13, 97]. The estimated CCT value for the optimized NBZPBPr<sub>0.1</sub> glass is 1737 K, which is lower than 5000 K. This indicates that the prepared NBZPBPr glass emits warm light. Additionally, the color purity (CP) of the prepared

NBZPBPr glasses is determined and the evaluated CP value for the optimized NBZPBPr<sub>0.1</sub> glass is 97.0% [13]. Hence, the aforementioned parameters validate that the NBZPBPr<sub>0.1</sub> glass can be suitable for use in orange-red components of white LED and other optoelectronic applications.

### 3.6. Effect of temperature on the emission intensity of the NBZPBPr Glass

In order to examine the influence of temperature on emission and assess the thermal stability of the glass, a study was conducted on 0.1 mol% Pr<sup>3+</sup> doped NBZPB (NBZPBPr<sub>0.1</sub>) under the excitation wavelength of 446 nm with varying temperature profiles from 303 K to 473 K, as shown in Fig. 3.9.

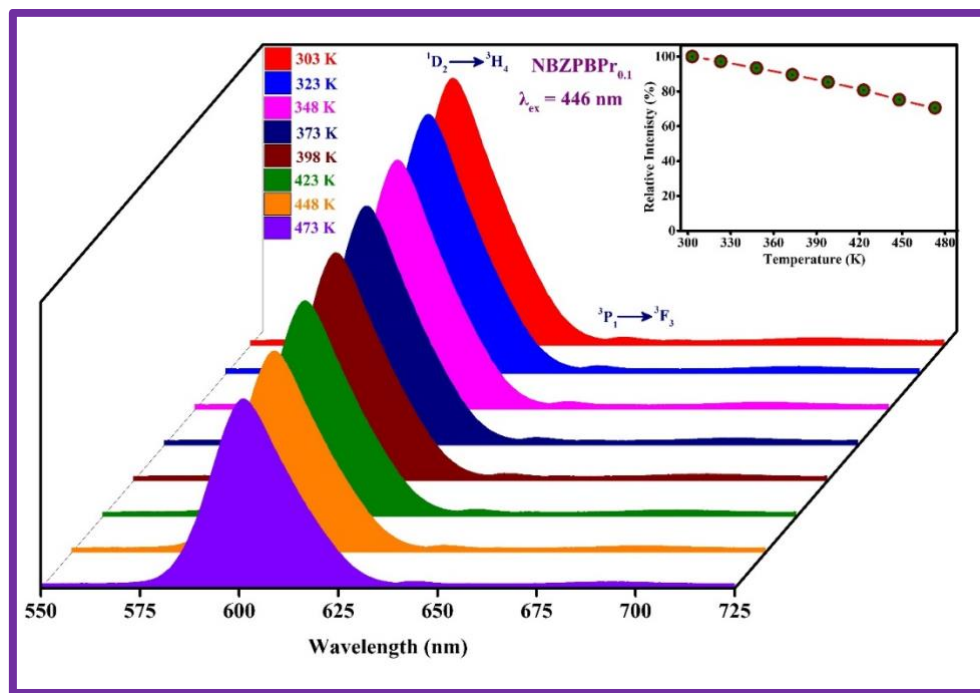


**Fig. 3.9.** Temperature-dependent PL spectra for the optimized NBZPBPr<sub>0.1</sub> glass sample with temperature varying from 303 K to 473 K under 446 nm excitation wavelength. [Inset represents the relative emission intensity variation with varying temperatures from 303 K to 473 K.

The emission intensity of the NBZPBPr0.1 glass decreases gradually without any change in the peak position as the temperature increases from 303 K to 473 K. The temperature dependence along with the relative intensity of the prepared glass under blue excitation is illustrated in the inset of Fig. 3.9. The emission intensity of the NBZPBPr0.1 glass was maintained at 89.53% at 373 K (100 °C) and 75.17% at 423 K (150 °C), compared to the initial emission intensity at 303 K, which suggest that the prepared glasses have excellent thermal stability. Activation energy ( $\Delta E_a$ ) is also another major parameter used for determining the thermal stability of the prepared glasses and can be evaluated with the help of the Arrhenius equation as reported in the literature [19].

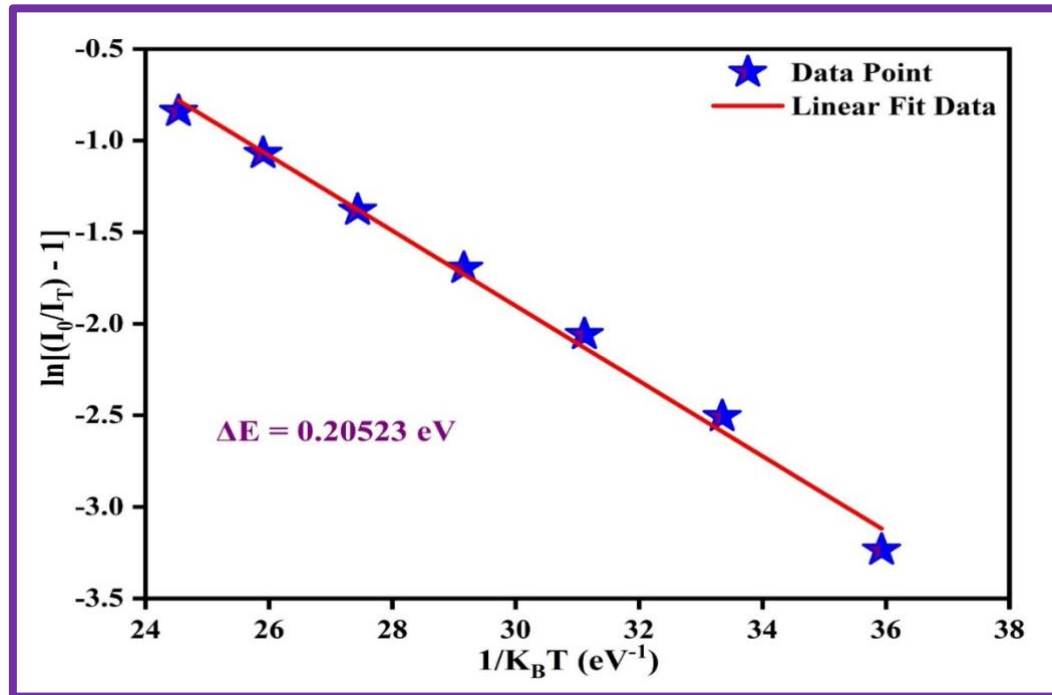


**Fig. 3.10.** Linear fitted plot between  $\ln[(I_0/I_T) - 1]$  versus  $1/K_B T$ .

The slope can be determined by analyzing the graph between  $\ln[(I_0/I_T) - 1]$  versus  $1/K_B T$  from Fig. 3.10 and calculating the activation energy. The observed value is found to be 0.205 eV, indicating outstanding thermal stability of the glass.

## Chapter 4: Conclusion and Future Scope of the Work

---

### 4.1. Conclusions

Transparent NBZPB glasses with varying  $\text{Pr}^{3+}$  ion concentrations were formed through the melt-quenching method. In order to comprehend their functionality in optoelectronic applications, various characterization techniques, such as DSC, XRD, FT-IR, optical absorption, photoluminescence and temperature-dependent PL were deployed. The absence of crystalline peaks in the diffraction profiles authorizes the amorphous character of the prepared glasses. Whereas, FT-IR spectroscopy assists in determining the various functional linkages of the prepared glass host. The optical characteristics (indirect allowed  $E_{opt}$  and  $n$ ) of the NBZPBPr<sub>0.1</sub> glass matrix were computed with optical absorption data. The emission spectral profiles of the prepared  $\text{Pr}^{3+}$  embedded NBZPB glass matrices exhibit an intense orange-red emission peak at 602 nm in the visible region when excited by a blue wavelength of 446 nm. The optimal content of the dopant ions in the formed NBZPBPr glasses has been obtained to be 0.1 mol%. Additionally, the temperature-dependent PL spectral profiles indicate the remarkable thermal stability of the NBZPBPr glass, along with a high activation energy value. The aforementioned findings validate that the orange-red emitting  $\text{Pr}^{3+}$  induced NBZPB glasses can be a promising candidate for optoelectronic applications.

### 4.2. Future Scope of the work

- To enhance the photoluminescence properties using co-dopants/flux and to fabricate a prototype w-LED using the optimized glass.
- To study in detail, the energy transfer studies and various colourimetric/photometric properties of the optimized glass for solid-state lighting applications.

- Future work can show different dopants/co-dopants improving the thermal stability of the glass, which can further improve quantum efficiency.
- To publish research papers in internationally reputed scientific journals and present papers at International and National conferences.

## References

- [1] E. Erol, N. Vahedigharehchopogh, O. Kırışlı, M. Ç. Ersundu, A. E. Ersundu, *J. Phys.: Condens. Matter* 33 (2021) 483001.
- [2] A. De Almeida, B. Santos, P. Bertoldi, M. Quicheron, *Renew. Sustain. Energy Rev.* 34 (2014) 30–48.
- [3] I. L. Azevedo, M. G. Morgan, F. Morgan, *Proc. IEEE*, vol. 97 (2009) 481–510.
- [4] N. U. Islam, M. Usman, T. Jamil, *Energy Policy* 160 (2022) 112676.
- [5] N. O. Etafo, *Curr. Phys.* 01 (2024) 2772-3356.
- [6] V. C. Bender, T. B. Marchesan, J. M. Alonso, *IEEE Ind. Electron. Mag.* 9 (2015) 6–16.
- [7] J. Cho, J. H. Park, J. K. Kim, E. F. Schubert, *Laser Photon. Rev.* 11 (2017) 1600147.
- [8] V. Kumar, S. Kumari, S. Malik, Ravita, T. Sharma, A. Prasad, A. S. Rao, *J. Fluoresc.* (2025).
- [9] P. Kumar, S. Singh, I. Gupta, A. Dalal, V. Kumar, D. Singh, *Mater. Sci. Eng.: B* 288 (2023) 116189.

- [10] A. Nardelli, E. Deuschle, L. D. de Azevedo, J. L. N. Pessoa, and E. Ghisi, *Renew. Sustain. Energy Rev.* 75 (2017) 368–379.
- [11] T. Erdem, A. Orenc, D. Akcan, F. Duman, Z. Soran-Erdem, *RSC Adv.* 14 (2024) 18528–18535.
- [12] P. Meejitpaisan, W. Wongwan, J. Kaewkhao, in *J. Phys.: Conf. Ser.* 1259 (2019) 012004.
- [13] Vikas, M. Jayasimhadri, *Luminescence* 37 (2022) 2059–2066.
- [14] D. Karunatilaka, F. Zafar, V. Kalavally, R. Parthiban, *IEEE Commun. Surv. Tutor.*, 17 (2015) 1649–1678.
- [15] S. T. Tan, X. W. Sun, H. V. Demir, S. P. Denbaars, *IEEE J. Photonics* 4 (2012) 613–619
- [16] S. Tiwari, J. V. Yakhmi, *Defect Diffus. Forum* 361 (2015) 15–68.
- [17] C. Pravallika, K. Swapna, I. S. Deo, Sk. Mahamuda, M. Venkateswarulu, A. S. Rao, V. P. G., *J. Fluoresc.* 35 (2025) 701–721.
- [18] V. Sangwan, V. Siwach, M. K. Sahu, I. Maurya, M. Jayasimhadri, D. Haranath, *Mater. Today Proc.* (2024) 1–7.
- [19] Vikas, M. Jayasimhadri, D. Haranath, *Int. J. Appl. Glass. Sci.* 13 (2022) 645–654.
- [20] A. U. Ahmad, F. K. Yam, S. Hashim, S. K. Ghoshal, A. Abdulhameed, *Opt. Quantum Electron.* 56 (2024) 1152.
- [21] J. Xu, S. Liu, Y. Wang, X. Cai, Y. Lu, Y. Chen, *J. Mater. Sci.: Mater. Electron.* 35 (2024) 397.
- [22] C. Kumari, R. Gopal, H. Yadav, J. Manam, *J. Mater. Sci.: Mater. Electron.* 35 (2024) 638.

- [23] S. Kaur, A. K. Vishwakarma, N. Deopa, A. Prasad, M. Jayasimhadri, A. S. Rao, *Mater. Res. Bull.* 104 (2018) 77–82.
- [24] M. Vikas, D. Jayasimhadri, Haranath, *J. Lumin.* 266 (2024) 120276.
- [25] Vikas, M. Jayasimhadri, D. Haranath, *Curr. Appl. Phys.* 58 (2024) 11–20.
- [26] I. Kumar, A. Kumar, S. Kumar, V. Sangwan, A. K. Gathania, *IEEE Photonics J.* 16 (2024) 1–7.
- [27] P. C. Ricci, *Crystals* 10 (2020) 559.
- [28] V. Hegde, *Appl. Phys. A Mater. Sci. Process.* 129 (2023) 25.
- [29] V. H. Rao, P. S. Prasad, K. S. Babu, *Opt. Mater. (Amst)* 101 (2020) 109740.
- [30] A. I. Voloshin, N. M. Shavaleev, V. P. Kazakov, *J. Lumin.* 93 (2001) 199–204.
- [31] M. Aygün, Z. Aygün, F. A. Celik, E. Karabulut, M. Yilmaz, *Adv. Theory. Simul.* 7 (2024) 2400376.
- [32] A. R. Varghese, A. Jose, T. Krishnapriya, A. George, J. R. Jose, A. Gopinath, C. Joseph, P. R. Biju, *J. Mater. Sci.: Mater. Electron.* 33 (2022) 20204–20222.
- [33] R. D. Dupuis, M. R. Krames, *J. Lightwave Technol.* 26 (2008) 1154–1171.
- [34] I. Akasaki, *J. Cryst. Growth* 300 (2007) 2–10.
- [35] J. Cho, J. H. Park, J. K. Kim, E. F. Schubert, *Laser Photon Rev.* 11 (2017) 1600147.
- [36] J. M. Fernández-Navarro, M. Á. Villegas, *Modern Methods for Analysing Archaeological and Historical Glass, Volume I* 1 (2013) 1–22.
- [37] T. Dilova, G. Atanasova, A. O. Dikovska, N. N. Nedyalkov, *Appl. Surf. Sci.* 505 (2020) 144625.

- [38] J. E. Shelby, *Intro. Glass Sci. Technol.*, 2nd ed., R. Soc. Chem., Cambridge (2005).
- [39] P. Badrinarayanan, W. Zheng, Q. Li, S. L. Simon, *J. Non. Cryst. Solids* 353 (2007) 2603–2612.
- [40] K. V. R. Murthy, H. S. Virk, *Trans Tech Publications Ltd.* 347 (2014) 1-34.
- [41] Zwinkels J.C., ‘Luminescence’1929, *Encycl. Color Sci. Technol.*, 2nd ed., R. Shamey (ed.), Springer Science, 2020.
- [42] N. Hussain, I. Ayoub, U. Mushtaq, R. Sehgal, S. Rubab, R. Sehgal, H. C. Swart, V. Kumar, in *Rare-Earth-Activated Phosphors: Chemistry and Applications*, Elsevier 3–41 (2022).
- [43] J. R. Lakowicz, *Principles of Fluorescence Spectroscopy* 3<sup>rd</sup> Ed. pp. 1–954 (2006).
- [44] S. M. Sze, Yiming. Li, and K. Kwok. Ng, ‘Physics of semiconductor devices’, 4<sup>th</sup> Ed. pp. 931 (2021).
- [45] V. I. Klimov, *J. Phys. Chem. B* 104 (2000) 6112–6123.
- [46] J. R. Lakowicz, in *Principles of Fluorescence Spectroscopy* 3<sup>rd</sup> Ed. pp. 27-61 (2006).
- [47] T. Kirchartz, J. A. Márquez, M. Stolterfoht, T. Unold, *Adv. Energy Mater.* 10 (2020) 1904134.
- [48] S. O. Adeleye, A. A. Adeleke, P. Nzerem, A. I. Olosho, E. N. Anosike-Francis, T. S. Ogedengbe, P. P. Ikubanni, R. A. Saleh, J. A. Okolie, *Trends Sci.* 21 (2024) 8759.
- [49] S. N. Rasool, S. Shabeena, N. Kiran, *J. Mater. Sci.: Mater Electron.* 33 (2022) 25187–25197.
- [50] S. S. Deol, P. Kaur, J. Singh, P. Kaur, Y. K. Vermani, T. Singh, *J. Phys. Conf. Ser.* 2426 (2023) 012034.




- [51] S. C. Colak, G. Kilic, *J. Mater. Sci.: Mater. Electron.* 33 (2022) 21852–21863.
- [52] V. Prajzler, O. Lyutakov, I. Huttel, J. Oswald, V. Jerabek, *Adv. Lasers Electro Opt.*, pp. 59-68 (2010).
- [53] G. Anjaiah, S. K. Nayab Rasool, P. Kistaiah, *J. Lumin.* 159 (2015) 110–118.
- [54] B. Zheng, J. Fan, B. Chen, X. Qin, J. Wang, F. Wang, R. Deng, X. Liu, *Chem. Rev.* 122 (2022) 5519–5603.
- [55] L. Wang, R. J. Xie, T. Suehiro, T. Takeda, N. Hirosaki, *Chem. Rev.* 118 (2018) 1951–2009.
- [56] G. A. Alharshan, M. I. Elamy, N. M. Ebrahim, A. M. A. Mahmoud, Y. S. Rammah, R. A. Elsad, M. H. Misbah, S. A. Said, *Opt. Quantum Electron.* 56 (2024) 1179.
- [57] N. A. M. Alsaif, N. Alfryyan, H. Al-Ghamdi, A. M. Abdelghany, M. S. Sadeq, A. S. Abouhaswa, A. M. Alanazi, Y. S. Rammah, *Opt. Quantum Electron.* 56 (2024) 950.
- [58] R. Pagoti, S. Panda, V. Patchapureddy, R. K. Padhi, B. Subramanian, H. Jena, B. S. Panigrahi, *Luminescence* 36 (2021) 1706–1715.
- [59] U. Hoppe, P. T. Freudenberger, R. K. Brow, J. Bednarcik, A. C. Hannon, *Solids* 5 (2024) 355-374.
- [60] S. Ibrahim, M. Abdel-Baki, F. El-Diasty, *Optical Engineering* 51 (2012) 093401–1.
- [61] X. G. Pang, T. Y. Eeu, P. M. Leong, W. N. Wan Shamsuri, R. Hussin, *Adv. Mat. Res.* 895 (2014) 280–283.
- [62] I. Kostova, *J. Chem. Technol. Metall.* 55 (2020) 354-358.
- [63] K. Alkhamis, H. A. Alghasham, A. Almahri, H. Alessa, O. A. Osra, S. S. Al-Ghamdi, A. M. Binyaseen, N. M. El-Metwaly, *Arab. J. Chem.* 17 (2024) 105875.


- [64] A. Ichoja, S. Hashim, S. K. Ghoshal, I. H. Hashim, R. S. Omar, *J. Rare Earths* 36 (2018) 1264–1271.
- [65] M. I. Sayyed, A. H. Almuqrin, *Silicon* 16 (2024) 3777–3784.
- [66] A. A. Bunaciu, E. gabriela Udriștioiu, H. Y. Aboul-Enein, *Taylor and Francis Ltd.* 45 (2015) 289-299.
- [67] S. A. Khan, S. B. Khan, L. U. Khan, A. Farooq, K. Akhtar, A. M. Asiri, *Handbook of Materials Characterization* 317–344 (2018).
- [68] S. K. Sharma, D. S. Verma, L. U. Khan, S. Kumar, S. B. Khan, *Handbook of Materials Characterization* 1–613 (2018).
- [69] M. Abdi-Jalebi, M. Ibrahim Dar, A. Sadhanala, E. M. J. Johansson, M. Pazoki, *Characterization Techniques for Perovskite Solar Cell Materials* 49–79 (2020).
- [70] J. Jimenez, J. W. Tonn, *Springer Ser. Opt. Sci.* 202 (2016) 143–211.
- [71] C. A. T. Laia, A. Ruivo, in book *Fluorescence in Industry*, 18 (2019) 365–388.
- [72] M. Gaft, R. Reisfeld, G. Panczer, ‘Modern Luminescence Spectroscopy of Minerals and Materials’, (2015).
- [73] D. Manzani, J. F. D. S. Petrucci, K. Nigoghossian, A. A. Cardoso, S. J. L. Ribeiro, *Scientific Reports* 7 (2017) 1–11.
- [74] C. Robert, D. Lagarde, F. Cadiz, G. Wang, B. Lassagne, T. Amand, A. Balocchi, P. Renucci, S. Tongay, B. Urbaszek, X. Marie, *Phys. Rev. B.* 93 (2016) 205423.
- [75] Y. Kanemitsu, *J. Mater. Chem. C. Mater.* 5 (2017) 3427–3437.
- [76] M. V. Sasi kumar, B. Rajeswara Reddy, S. Babu, A. Balakrishna, Y. C. Ratnakaram, *J. Taibah Univ. Sci.* 11 (2017) 593–604.

- [77] N. T. El-Shamy, E. M. Mahrous, S. K. Alghamdi, M. J. Tommalieh, E. A. Rabie, H. M. Abomostafa, D. E. Abulyazied, A. S. Abouhaswa, *Inorg. Chem. Commun.* 164 (2024) 112437.
- [78] H. George, N. Deopa, S. Kaur, A. Prasad, M. Sreenivasulu, M. Jayasimhadri, A.S. Rao, *J. Lumin.* 215 (2019) 116693.
- [79] S. Vidya Sagar, S. Venkata Rao, S. Babu, S. K. Annar, *J. Opt. (India)* 53 (2024) 1-17.
- [80] R. Ravita, A. Prasad, P. Rohilla, R. Bajaj, A. Mor, R. Punia, A. S. Rao, *J. Fluoresc.* 34 (2024) 1783–1792.
- [81] Dr. G. Ramadevudu, M. N. Chary, *Glob. J. Sci. Front. Res.* 12 (2012) 41–46.
- [82] N. J. Kim, S. H. Im, D. H. Kim, D. K. Yoon, B. K. Ryu, *Electron. Mater. Lett.* 6 (2010) 103–106.
- [83] A. M. A. Mostafa, M. A. M. Uosif, Z. A. Alrowaili, R. Elsaman, A. A. Showahy, Y. B. Saddeek, S. A. M. Issa, A. Ene, H. M. H. Zakaly, *Materials* 14 (2021) 6632.
- [84] V. Ravi Teja, M. Sreenivasulu, V. K. Chavan, *J. Mater. Sci.: Mater. Electron.* 35 (2024) 166.
- [85] M. A. Marzouk, F. H. ElBatal, N. A. Ghoneim, F. M. Ezz-ElDin, *Silicon* 10 (2018) 959–965.
- [86] I. Bulus, S. A. Dalhatu, M. Isah, R. Hussin, E. A. Soje, *Sci. World J.* 12 (2017) 98–101.
- [87] N. A. M. Alsaif, H. I. Alrebdi, Y. S. Rammah, M. S. Shams, *J. Mater. Sci.: Mater. Electron.* 34 (2023) 1914.
- [88] S. H. Bindu, T. R. Rao, C. L. Raju, *Phys. Scr.* 90 (2015) 065802.

- [89] G. Ramadevudu, S. R. L. Srinivasa, M. S. A. Hameed, M. C. Narasimha, *Int. J. Eng. Sci. Techno.* 3 (2011) 6998-7005.
- [90] G. Mahajan, M. V. V. K. S. Prasad, K. Swapna, K. Seshulatha, M. Venkateswarulu, Sk. Mahamuda, A. S. Rao, *J. Mater. Sci.: Mater. Electron.* 35 (2024) 2055.
- [91] W. T. Carnall, G. L. Goodman, K. Rajnak, R. S. Rana, *J. Chem. Phys.* 90 (1989) 3443–3457.
- [92] W. T. Carnall, P. R. Fields, K. Rajnak, *J. Chem. Phys.* 49 (1968) 4424–4442.
- [93] V. Sangwan, M. Jayasimhadri, D. Haranath, *J. Mol. Struct.* 1322 (2025) 140577.
- [94] V. Dimitrov, S. Sakka, *J. Appl. Phys.* 79 (1996) 1736–1740.
- [95] M. A. Marzouk, I. M. Elkashef, A. M. Fayad, H. A. Elbatal, *J. Mater. Sci.: Mater. Electron.* 29 (2018) 10561–10572.
- [96] B. Klimesz, W. Ryba-Romanowski, R. Lisiecki, *Molecules* 29 (2024) 3041.
- [97] V. Siwach, M. Jayasimhadri, *Phys. Scr.* 99 (2024) 105009.

## Plagiarism Report

 Page 1 of 49 - Cover Page Submission ID trnoid::27535:99730932

**Tushar**  
**Tushar Thesis.docx**  
 Delhi Technological University

**Document Details**

Submission ID  
trnoid::27535:99730932

Submission Date  
Jun 7, 2025, 10:27 AM GMT+5:30

Download Date  
Jun 7, 2025, 10:29 AM GMT+5:30


File Name  
Tushar Thesis.docx

File Size  
3.6 MB

43 Pages

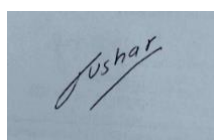
8,747 Words

50,727 Characters

 Page 1 of 49 - Cover Page Submission ID trnoid::27535:99730932

Place: Delhi

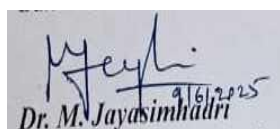
Date: 9 June 2025



**TUSHAR SINGH**

**23/MSCPHY/88**

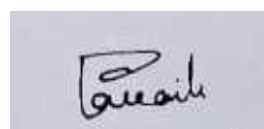
**Signature of Supervisor**



Dr. M. Jayasimhadri

**Dr. M. Jayasimhadri**

*Supervisor & Associate Professor  
Department of Applied Physics  
Delhi Technological University  
Delhi-110 042, India*



**Dr. K. Pavani**

*Joint-supervisor & Research Professor  
Department of Physics & I3N  
University of Aveiro  
Aveiro- 3810-193, Portugal*

## 10% Overall Similarity

The combined total of all matches, including overlapping sources, for each database.




### Filtered from the Report

- Small Matches (less than 10 words)

#### Match Groups

- 64 Not Cited or Quoted 9%**  
Matches with neither in-text citation nor quotation marks
- 1 Missing Quotations 0%**  
Matches that are still very similar to source material
- 2 Missing Citation 0%**  
Matches that have quotation marks, but no in-text citation
- 0 Cited and Quoted 0%**  
Matches with in-text citation present, but no quotation marks

#### Top Sources

- 5%  Internet sources
- 4%  Publications
- 5%  Submitted works (Student Papers)

#### Integrity Flags

##### 0 Integrity Flags for Review

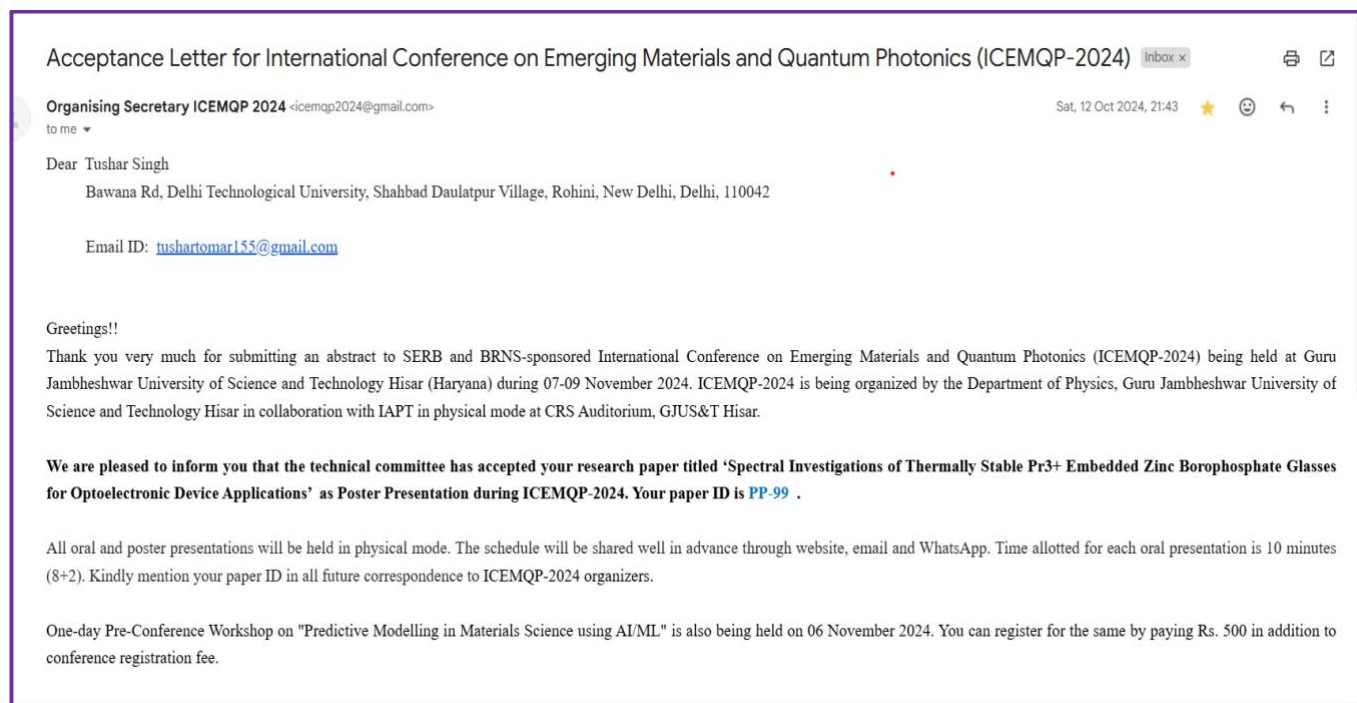
No suspicious text manipulations found.

Our system's algorithms look deeply at a document for any inconsistencies that would set it apart from a normal submission. If we notice something strange, we flag it for you to review.

A flag is not necessarily an indicator of a problem. However, we'd recommend you focus your attention there for further review.

## Conference Proof

### 1. Conference Acceptance Proof



### 2. Conference Participation Certificate





PP-99

**Spectral Investigations of Thermally Stable Pr<sup>3+</sup> Embedded Zinc Borophosphate Glasses for Optoelectronic Device Applications**

**Tushar Singh<sup>1</sup>, M. Jayasimhadri <sup>\*1</sup>, K. Pavani<sup>2</sup>**

<sup>1</sup>Luminescent Materials Research Lab (LMRL), Department of Applied Physics, Delhi Technological University, Bawana Road-110 042, India

<sup>2</sup>Department of Physics & I3N, University of Aveiro, 3810-193, Aveiro, Portugal

<sup>\*</sup>E-mail: jayasimha@dtu.ac.in

**Abstract**

Transparent Pr<sup>3+</sup> embedded zinc borophosphate (BZNBPPr) glasses have been prepared using the melt quenching procedure and their characterizations, including thermal, optical and photoluminescent features were studied in detail. The thermal stability of the BZNBPPr glass host matrix was determined via thermogravimetric-differential scanning calorimetry (TG-DSC) analysis. The non-crystalline/ amorphous behaviour of titled glass samples was confirmed using an X-ray diffraction (XRD) pattern. Moreover, the emission spectra of the prepared Pr<sup>3+</sup> embedded BZNBPr glass matrices exhibit two emission peaks in the visible region under blue (446 nm) excitation wavelength [1]. The chromaticity properties such as color purity (CP), correlated color temperature (CCT) and color coordinates of the prepared glasses were estimated using the emission spectra [2]. Furthermore, the temperature-dependent photoluminescence (TDPL) analysis has revealed that the titled glass matrix has good thermal stability. The above-mentioned results confirmed that the prepared Pr<sup>3+</sup> induced BZNBPr glasses can be potential candidates for optoelectronic device applications.

**Keywords:** Borophosphate glasses, X-ray diffraction, Photoluminescent analysis, TDPL studies

**References**

- [1] S. Liu, Y. Sun, S. Yan, Z. Zheng, *Solid State Sci.*, 134, 107056 (2022).
- [2] D. Ding, J. Gao, S. Zhang, L. Duo, *J. Lumin.*, 226, 117512 (2020).

Department of Physics, GJUS&T, Hisar